Mueller's dipole wave function in QCD: Emergent Koba-Nielsen-Olesen scaling in the double logarithm limit

Yizhuang Liu[*]
Institute of Theoretical Physics, Jagiellonian University, 30-348 Kraków, Poland

Maciej A. Nowak[†]
Institute of Theoretical Physics and Mark Kac Center for Complex Systems Research, Jagiellonian University, 30-348 Kraków, Poland

Ismail Zahed[‡]
Center for Nuclear Theory, Department of Physics and Astronomy, Stony Brook University, Stony Brook, New York 11794–3800, New York, USA

(Received 8 May 2023; accepted 18 July 2023; published 16 August 2023)

We analyze Mueller's QCD dipole wave function evolution in the double logarithm approximation (DLA). Using complex analytical methods, we show that the distribution of the dipole in the wave function (gluon multiplicity distribution) asymptotically satisfies the Koba-Nielsen-Olesen (KNO) scaling, with a nontrivial scaling function $f(z)$ with $z=\frac{n}{\bar{n}}$. The scaling function decays exponentially as $2(2.55)^2 z e^{-\frac{z}{0.3917}}$ at large z, while its growth is log-normal as $e^{-\frac{1}{2}\ln^2 z}$ for small z. A detailed analysis of the Fourier-Laplace transform of $f(z)$ allows for performing the inverse Fourier transform and accessing the nonasymptotic bulk region around the peak. The bulk and asymptotic results are shown to be in good agreement with the measured hadronic multiplicities in DIS, as reported by the H1 Collaboration at HERA in the region of large Q^2. A numerical tabulation of $f(z)$ is included. Remarkably, the same scaling function is found to emerge in the resummation of double logarithms in the evolution of jets. Using the generating function approach, we show why this is the case. The absence of KNO scaling in noncritical and super-renormalizable theories is briefly discussed. We also discuss the universal character of the entanglement entropy in the KNO scaling limit and its measurement using the emitted multiplicities in DIS and e^+e^- annihilation.

DOI: 10.1103/PhysRevD.108.034017

I. INTRODUCTION

In a broad and general sense, the high-energy limit of QCD is nontrivial. In the simplest case of e^+e^- annihilation, asymptotic freedom is sufficient to guarantee a controlled $\ln^{-1}\frac{Q^2}{\Lambda^2_{\rm QCD}}$ expansion in leading power [1,2]. However, there are a number of examples where the running coupling constant is not the only source of large logarithms. Remarkably, a complete understanding of the high-energy limit in these situations is still challenging, fifty years after the discovery of asymptotic freedom.

One important example which is relatively easy to understand is the Bjorken limit [3] of processes such as DIS [4] and DVCS [5] at moderate parton x, where it is commonly accepted [6,7] that in the leading power, the structure functions (or at least its moments) can be factorized into IR-sensitive matrix elements times hard coefficients in a way that can be cast into a controlled large-Q^2 expansion of the form $\alpha(Q)^{\frac{\gamma_1}{\beta_0}}(1+\mathcal{O}[\alpha(Q)])c_n$ with the help of the renormalization group equation (RGE). A more challenging situation is the Regge limit or small-x limit, where there are rapidity logarithms of the type $\ln\frac{1}{x}$, that cannot be systematically controlled by the RGE formalism. Nevertheless, if one is only interested in resumming the "leading logarithms" $\alpha_s^n \ln^n\frac{1}{x}$ in pQCD (assuming all the $k_\perp$'s are large), then major progresses have been made. In particular, the leading rapidity logarithms in the light-front wave functions (LFWFs) of a color dipole (Mueller's dipole) can be effectively extracted using Mueller's evolution equation [8,9]. This is essentially a cascade formed

[*]yizhuang.liu@uj.edu.pl
[†]maciej.a.nowak@uj.edu.pl
[‡]ismail.zahed@stonybrook.edu

by consecutive small-x gluon emissions ordered in rapidity. From Mueller's dipole, many other evolution equations, such as the linearized BFKL equation[1] for the gluon density [10–12] or its BK variant [13,14] for the cross section, can be derived under further assumptions.

Nevertheless, whether the small-x pQCD evolutions present a correct and self-consistent description of the Regge limit is still not clear. It is well known that the BFKL evolution mixes different "twists" and tends to "diffuse" into soft regions, which is made worse by the "IR renormalon" caused by running inside massless integrals. It is also well known that the derivation of the famous Froissart bound relies crucially on the existence of an exponential decay at a large impact parameter, a feature that is essentially nonperturbative. The popular assumption is that there will be an emergent "saturation scale" Q_s that is hard enough to justify pQCD at large rapidity or small x, due to ever-increasing gluon density. As a result, the confinement problem can be avoided. The "color-glass condensate" (CGC) approach [15–18] to gluon saturation is based on this assumption. The string-gauge duality provides another way to look at the Regge limit at strong coupling (large impact parameter or small Q^2). It has been proposed that the small dipoles are string bits [19–21], and their evolution is best captured by a dual string [22–26]. In Refs. [26,27], a string-based holographic Reggeization formalism in which forward dipole-dipole scattering is realized as the exchange-minimal surfaces in appropriate geometries has been proposed and agrees qualitatively with Mueller's approach [8,9] in the conformal limit. In the large-impact-parameter limit, due to the presence of a natural string tension, the approach fulfills the Froissart bound in a nonperturbative manner.

Among all the features of the small-x evolution, the growth of the "parton number" with rapidity plays a key role. In Mueller's dipole picture, the LFWF of the projectile dipole tends to split into more and more dipoles ordered strongly in rapidity, before interacting with the target. The large number of color charges present in the wave function should be responsible for the large amount of observed particle multiplicity [28]. The distribution of the virtual dipoles in Mueller's wave function in the "diffusion limit" has long been believed to be similar to the simplified $0+1$D reduction [9,29,30], which satisfies the famous KNO scaling [31,32], with a "geometric" scaling function e^{-z}. However, this scaling function differs significantly from the observed scaling function for ep data [28]. On the other hand, the dipole evolution has another limit, which actually forms the common region with the DGLAP evolution [33], the double logarithm approximation (DLA) limit. In this limit, the growth of the gluon density is much slower; however, as we will show in this paper, the distribution of dipoles in the wave function displays a nontrivial scaling function, in agreement with the reported hadronic multiplicities by the H1 Collaboration at HERA [28].

It has been suggested [34,35] that underlying the large number of observed particle multiplicity is the onset of a quantum or entanglement entropy. In Refs. [30,35], the authors argued that Mueller's wave function is strongly entangled in longitudinal momentum space on the light front. This entanglement is distinct from the spatial entanglement, usually encoded in the ground-state wave function in the rest frame [36–40]. In the large-rapidity y limit, this entanglement is universally captured by an entropy $S=\ln\bar{n}\sim y$, where the mean multiplicity $\bar{n}\sim e^{\#y}$ grows exponentially, as noted in the dual string [34] and Mueller's cascade [35]. These observations have attracted a number of recent studies, both theoretically [29,30,41–50] and empirically [51–53]. For completeness, we note that a classical thermodynamical entropy using the production of gluons at high energy was initially explored in Ref. [54].

Recently, in Refs. [47,49], we have formalized the *rapidity space entanglement* between fast and slow degrees of freedom in Mueller's dipole, and derived a Balitsky-Kovchegov (BK) type equation for the associated reduced density matrix in the large-N_c limit. We have shown explicitly that for both the $0+1$D reduction and the $1+2$D QCD, the eigenvalues of the *reduced density matrix* indeed coincide with the dipole distribution. As a result, we have shown that the multiplicity entropy is of quantum nature. In particular, in the $0+1$D reduction, the dipole multiplicities follow a simple exponential distribution as in Ref. [9], while in the nonconformal QCD in $1+2$ dimensions, the mean dipole multiplicities were found to follow a Poisson distribution $p_n=e^{-\bar{n}}\bar{n}^n/n!$, with a linear growth of mean multiplicity with rapidity. The quantum entanglement entropy at large rapidity asymptotes at $S=\frac{1}{2}\ln\bar{n}\sim\frac{1}{2}\ln y$, which is much smaller than in $0+1$D reduction. The cascade of dipoles in $1+2$D dimensions is "quenched" kinematically by transverse integrals and provides a simple mechanism for saturation.

The solution of the evolved BK-type equations for the density matrix, and the underlying multiplicity of the emitting dipoles for QCD in $1+3$ dimensions, is not known except in the diffusion limit [9,29,30]. Needless to say, these dipole or gluon multiplicities, when released in a prompt ep or pp collision at high energy, are of relevance to the measured hadronic multiplicities. The purpose of this paper is to address this open problem partially, by solving directly Mueller's evolution in the double logarithm approximation (DLA), which resums the large $\ln\frac{1}{x}$ and large $\ln\frac{Q^2}{\Lambda^2_{\rm QCD}}$ simultaneously. This allows for an explicit derivation of the small dipole distributions, which will turn

[1]Notice that the BFKL equation is more universal than Mueller's dipole. Indeed, the BFKL spectrum is related to analytical continuation in anomalous dimensions of twist-2 operators, and is therefore generalizable to $\mathcal{N}=4$ SUSY CFT at a generic gauge coupling.

out to be in good agreement with the currently available H1 data from DIS scattering at HERA [28]. It also provides for an estimation of the entanglement entropy for DIS scattering in QCD, a measure of gluon decoherence, and possibly saturation. We should emphasize that the DLA limit lies in the common region of DGLAP evolution and Mueller's evolution. Hence, all the results in this paper can also be derived using the wave function evolution [33,55], underlying the DGLAP equation as well.

It is worth noting that the scaling function we established for Mueller's wave function evolution appears in the context of jet evolution [56,57]. In fact, this is not a coincidence, as we will detail below, and it follows from the BMS-BK correspondence, that maps the IR divergences in e^+e^- annihilation to the rapidity divergences in the dipole's wave function [58–62]. In leading order, this follows from the fact that all the leading IR logarithms are generated by a Markov process of consecutive emission of soft gluons, strongly ordered in energy into the asymptotic final-state cuts, in a way very similar to the underlying branching process of Mueller's dipole. At leading order, the two evolutions are related by a conformal transformation [63,64], which maps light-like dipoles to Wilson-line cusps, and virtual soft gluons in LFWF to real gluons in asymptotic states. The BMS evolution has a natural double logarithm limit corresponding to the Sudakov double logarithm in the virtual part (form factor), which can be obtained by imposing angular ordering on the emitted soft gluons. Through a conformal transformation, the angular ordering maps to the dipole size ordering. As a result, the scaling functions of the two DL limits are identical. These observations allow us to extend the concept of entanglement to jet evolution as well.

The organization of the paper is as follows: In Sec. II, we simplify Mueller's evolution equation for the generating functional in the DLA limit. We show that the resulting generating function in the DLA limit satisfies a second-order nonlinear differential equation, similar but not equivalent to the Painlevé-III equation. For large mean multiplicities $\bar{n}$, this allows the determination of all the leading consecutive moments of the dipole distribution, through a second-order recursive hierarchy. We study the behavior of the moment sequence and show that the underlying multiplicity distribution obeys Koba-Nielsen-Olesen (KNO) scaling [31,32] in the form $p_n = \frac{1}{\bar{n}} f(\frac{n}{\bar{n}})$, with the scaling variable $z = n/\bar{n}$ in the large-$\bar{n}$ limit and the scaling function $f(z)$. In Sec. III, we show that the complex analytic Fourier-Laplace transform $Z(t)$ of the KNO scaling function $f(z)$ can be determined by analytically continuing from a simple integral representation, from which the $f(z)$ can be obtained by Fourier inversion. In particular, for large and small z, the asymptotic forms of $f(z)$ can be determined exactly, and for general z numerically. In Sec. IV, we compare our DLA scaling function $f(z)$ to the empirical charged multiplicity scaling function $\Psi(z)$ extracted from ep data at HERA [28], and we find good agreement. In Sec. V, we briefly review the leading-order BMS evolution equation, using the generating functional formalism of Ref. [8]. The relation to the dipole evolution is made manifest. In Sec. VI, we show that the ensuing multiplicities for both the wave function and jet evolutions are quantum entangled. The entanglement entropy asymptotes at $S = \ln \bar{n}$ in the DLA. The logarithmic growth of the entanglement entropy with $\bar{n}$ is generic for all hadronic multiplicities in QCD with KNO scaling. Our conclusions are given in Sec. VII. In the Appendix, we briefly discuss the multiplicity distributions of super-renormalizable theories and their lack of KNO scaling.

II. MUELLER'S DIPOLE WAVE FUNCTION AND ITS DLA LIMIT

In this section, we consider Mueller's dipole evolution equation in the DLA limit. We briefly recall that in Refs. [8,9] using the planar limit, it was shown that the consecutive emission of gluons with smaller and smaller x into the light-front wave function (LFWF) of a valence quark-antiquark pair (Mueller's dipole) leads to a closed equation for the generating functional of the squared norms of the LFWF:

$$\begin{aligned}\mathcal{Z}\left(b_{10},\frac{x_0}{x_{\min}},\lambda\right) &= S\left(b_{10},\frac{x_0}{x_{\min}}\right) + \lambda\frac{\alpha_s N_c}{2\pi^2}\int_{x_{\min}}^{x_0}\frac{dx_1}{x_1} \\ &\times S\left(b_{10},\frac{x_0}{x_1}\right)\int db_2^2\frac{b_{10}^2}{b_{12}^2 b_{20}^2} \\ &\times \mathcal{Z}\left(b_{12},\frac{x_1}{x_{\min}},\lambda\right)\mathcal{Z}\left(b_{20},\frac{x_1}{x_{\min}},\lambda\right),\end{aligned} \tag{1}$$

with the Sudakov or "soft factor" for "virtual" emissions[2] as

$$S\left(b_{10},\frac{x_0}{x_1}\right) = \exp\left[-\frac{\alpha_s N_c}{\pi}\ln b_{10}^2\mu^2\ln\frac{x_0}{x_1}\right]. \tag{2}$$

Z generates the probability of finding an $n+1$ dipole inside the LFWF of the $Q\bar{Q}$ pair:

$$\mathcal{Z}(b,y,\lambda) = \sum_{n=0}^{\infty}\lambda^n p_n(b,y). \tag{3}$$

[2]The use of the words "virtual" and "real" in the context of wave functions is not very precise. A more precise definition would be "disconnected" and "connected" contributions. This said, note that this contribution is the square of the standard transverse-momentum-dependent (TMD) soft factor, with one factor from the wave function and the other factor from the conjugate wave function.

Unitarity requires $Z=1$ for $\lambda=1$, which is manifest in Eq. (3). The *factorial moments*[3] of the distribution p follow as

$$\frac{d^k}{d\lambda^k}\mathcal{Z}(b,y,\lambda)|_{\lambda=1}=\sum_{n=0}^{\infty}n(n-1)..(n-k+1)p_n \equiv\langle n(n-1)\ldots(n-k+1)\rangle. \tag{4}$$

The knowledge of $\mathcal{Z}$ provides a detailed understanding of the LFWF of the $Q\bar{Q}$ pair in the small-x sector.

A. The double logarithm limit

The double logarithm limit (DLA) corresponds to the situation where b_2 is very close to either b_0 or b_1, the locations of the mother dipole, and so on with $0b_3\ldots$. As a result, the emitted dipoles carry smaller and smaller sizes. In this limit, if one introduced the scale parameter $\alpha=\ln\frac{b_{10}^2}{b^2}=\ln\frac{Q^2}{Q_0^2}$ where b is the size of the emitted dipole, which is identified as the inverse of Q, then the evolution equation simplifies to

$$\mathcal{Z}(y,\alpha,\lambda)=\exp\left[-\frac{\alpha_s N_c}{\pi}\alpha y\right]+\frac{\alpha_s N_c\lambda}{\pi}\int_0^{\alpha}d\alpha'\int_0^{y}dy' \times\exp\left[-\frac{\alpha_s N_c}{\pi}\alpha(y-y')\right]\mathcal{Z}(\alpha',y',\lambda)\mathcal{Z}(\alpha,y',\lambda). \tag{5}$$

It is easy to check that for $\lambda=1$, one has the trivial solution $\mathcal{Z}=1$. By taking the derivative with respect to y, one obtains the exact equation in DLA:

$$\frac{\partial\mathcal{Z}(\alpha,y)}{\partial y}=\frac{\alpha_s N_c}{\pi}\mathcal{Z}(\alpha,y)\left(-\alpha+\lambda\int_0^{\alpha}d\alpha'\mathcal{Z}(\alpha',y)\right). \tag{6}$$

On the other hand, for the mean $\bar{n}=\frac{d\mathcal{Z}}{d\lambda}|_{\lambda=1}$,

$$\frac{\partial\bar{n}}{\partial y}=\frac{\alpha_s N_c}{\pi}\left(\alpha+\int_0^{\alpha}\bar{n}(\alpha',y)d\alpha'\right), \tag{7}$$

$$\frac{\partial^2\bar{n}}{\partial y\partial\alpha}=\frac{\alpha_s N_c}{\pi}(\bar{n}+1)\sim\frac{\alpha_s N_c}{\pi}\bar{n}. \tag{8}$$

The second equation is nothing but the DGLAP evolution equation in the DLA limit for the gluon density, allowing the identification $\bar{n}=xG(x,Q^2)$.

[3]Sometimes they are also called the "disconnected moments" or "multiplicity correlators."

Note that for a running gauge coupling α_s,

$$\alpha_s(Q)=\frac{1}{\beta_0\ln\frac{Q^2}{\Lambda_{\rm QCD}^2}}\quad\text{and}\quad\gamma=\ln\frac{\ln\frac{Q^2}{\Lambda_{\rm QCD}^2}}{\ln\frac{Q_0^2}{\Lambda_{\rm QCD}^2}}, \tag{9}$$

where $\beta_0=\frac{1}{4\pi}\left(\frac{11N_c}{3}-\frac{2N_f}{3}\right)$, the above equations still hold, with

$$\mathcal{Z}(y,\gamma)=\exp\left[-\frac{N_c}{\pi\beta_0}y\gamma\right]+\lambda\frac{N_c}{\pi\beta_0}\int_0^{\gamma}d\gamma'\int_0^{y}dy' \times\exp\left[-\frac{N_c}{\pi\beta_0}(y-y')\gamma\right]\mathcal{Z}(y',\gamma')\mathcal{Z}(y',\gamma), \tag{10}$$

which is identical to Eq. (5) with the identification $\alpha_s\to\frac{1}{\beta_0}$ and $\alpha\to\gamma$. Below, we still use the notation in Eq. (5) with this understanding.

To investigate the multiplicity distribution in the DLA, we note that the generating function $\mathcal{Z}$ is only a function of ρ:

$$\rho=\frac{\alpha_s N_c}{\pi}y\ln\frac{Q^2}{Q_0^2},\quad\text{no running}, \tag{11}$$

$$\rho=\frac{N_c}{\pi\beta_0}y\ln\frac{\ln\frac{Q^2}{\Lambda_{\rm QCD}^2}}{\ln\frac{Q_0^2}{\Lambda_{\rm QCD}^2}},\quad\text{with running}, \tag{12}$$

which amounts to

$$\mathcal{Z}(\rho)=e^{-\rho}+\lambda\rho\int_0^1 dt_1\int_0^1 dt_2 e^{-\rho(1-t_2)}\mathcal{Z}(\rho t_1 t_2)\mathcal{Z}(\rho t_2) \tag{13}$$

in both cases. In particular, the equation for the averaged number of soft gluons, $\bar{n}=xG(x,Q)$, becomes

$$\rho\frac{d^2\bar{n}}{d\rho^2}+\frac{d\bar{n}}{d\rho}=\bar{n}+1. \tag{14}$$

The solution is given in terms of the Bessel I_0 function

$$\bar{n}(\rho)=I_0(2\sqrt{\rho})-1, \tag{15}$$

with the correct growth in rapidity at large y, in leading double-log accuracy [33].

To solve $\mathcal{Z}(\lambda)$ in general, we define $\mathcal{Z}=e^{\mathcal{W}}$, and the equation for $\mathcal{W}$ now becomes

$$\rho\frac{d^2\mathcal{W}}{d\rho^2}+\frac{d\mathcal{W}}{d\rho}=\lambda e^{\mathcal{W}}-1. \tag{16}$$

In terms of $u = 2\sqrt{\rho}$, one has

$$\frac{d^2\mathcal{W}}{du^2} + \frac{1}{u}\frac{d\mathcal{W}}{du} = (\lambda e^{\mathcal{W}} - 1), \tag{17}$$

which can be written as

$$\nabla^2\mathcal{W} = (\lambda e^{\mathcal{W}} - 1), \tag{18}$$

with ∇^2 being the radial part of the two-dimensional Laplacian. Note that in terms of the original generating function $\mathcal{Z}$, the equation is

$$\frac{d^2\mathcal{Z}}{d\rho^2} = \frac{1}{\mathcal{Z}}\left(\frac{d\mathcal{Z}}{d\rho}\right)^2 - \frac{1}{\rho}\frac{d\mathcal{Z}}{d\rho} + \frac{1}{\rho}(\lambda\mathcal{Z}^2 - \mathcal{Z}), \tag{19}$$

which resembles closely the third Painlevé equation (except for the last term in the last bracket).

B. Factorial moments n_k in the large-rapidity limit: The asymptotic moment sequence a_n

To gain more insight into the multiplicity distribution, in this section we investigate a property of the factorial moments, $n_k = \frac{d^k}{d\lambda^k}\mathcal{Z}|_{\lambda=1}$. Successive derivatives show that they satisfy the hierarchy

$$\rho\frac{d^2n_1}{d\rho^2} + \frac{dn_1}{d\rho} = n_1 + 1, \tag{20}$$

$$\rho\frac{d^2n_2}{d\rho^2} + \frac{dn_2}{d\rho} - n_2 = 2\rho\left(\frac{dn_1}{d\rho}\right)^2 + 2n_1^2 + 4n_1, \tag{21}$$

$$\begin{aligned}\rho\frac{d^2n_3}{d\rho^2} + \frac{dn_3}{d\rho} - n_3 = &-6\rho n_1\left(\frac{dn_1}{d\rho}\right)^2 + 6\rho\frac{dn_1}{d\rho}\frac{dn_2}{d\rho} \\ &+ 6n_2n_1 + 6n_1^2 + 6n_2,\end{aligned} \tag{22}$$

$$\begin{aligned}\rho\frac{d^2n_4}{d\rho^2} + \frac{dn_4}{d\rho} - n_4 = &24\rho n_1^2\left(\frac{dn_1}{d\rho}\right)^2 - 12\rho n_2\left(\frac{dn_1}{d\rho}\right)^2 \\ &- 24\rho n_1\frac{dn_1}{d\rho}\frac{dn_2}{d\rho} + 6\rho\left(\frac{dn_2}{d\rho}\right)^2 \\ &+ 8\rho\frac{dn_1}{d\rho}\frac{dn_3}{d\rho} + 8n_1n_3 + 6n_2^2 \\ &+ 24n_2n_1 + 8n_3,\end{aligned} \tag{23}$$

and so on. Here, $n_1 = \bar{n}$ is just the mean multiplicity. We would like to study the asymptotics of the above equations in the large-u limit. The solution $n_1 \sim e^{2\sqrt{\rho}} \sim e^u$ suggests that we can find the asymptotic solutions of the form $n_k \sim a_k e^{ku}$ in the large-u limit.

For this purpose, notice that in terms of $u = 2\sqrt{\rho}$, the derivative terms on the left-hand side of the equations reads

$$\rho\frac{d^2}{d\rho^2} + \frac{d}{d\rho} \equiv \frac{d^2}{du^2} + \frac{1}{u}\frac{d}{du}. \tag{24}$$

In the large-u limit, we only need to keep the $\frac{d^2}{du^2}$ term on the left-hand side and drop all terms that are exponentially suppressed on the right-hand side in order to obtain the *leading asymptotics* of the form

$$n_k|_{u\to\infty} \to a_k e^{ku}. \tag{25}$$

The above defines uniquely the *asymptotic moment sequence* a_n with the initial condition $a_0 = a_1 = 1$. The $a_0 = 1$ is due to the probability conservation, while $a_1 = 1$ fixes the overall normalization of the sequence. Defining

$$b_n = \frac{a_n}{n^2}, \tag{26}$$

it is easy to show that b_n satisfies the recursive relations

$$n^2 b_n = B_n(b_1, b_2, \ldots b_{n-1}, b_n). \tag{27}$$

Here, the B_n's are the complete Bell's polynomials, which are defined for a generic sequence b_n through the relation

$$\exp\left[\sum_{n=1}^{\infty}\frac{b_n u^n}{n!}\right] = 1 + \sum_{n=1}^{\infty}\frac{B_n(b_1, \ldots b_n)u^n}{n!}. \tag{28}$$

Notice that the Bell's polynomial satisfies the recursive relation

$$\begin{aligned}B_n(b_1, \ldots . b_n) = b_n + \sum_{i=0}^{n-2}&\frac{(n-1)!}{i!(n-1-i)!} \\ &\times B_{n-1-i}(b_1, \ldots b_{n-1-i})b_{i+1}\end{aligned} \tag{29}$$

for a generic sequence b_n. Given the above, Eq. (27) can be simplified to

$$(n^2 - 1)b_n = \sum_{i=0}^{n-2}\frac{(n-1)!}{i!(n-1-i)!}(n-1-i)^2 b_{n-1-i}b_{i+1}, \tag{30}$$

which can be transformed to match Refs. [56,57]. Using this, the first few terms are readily generated as

$$a_2 = \frac{4}{3}, \quad a_3 = \frac{9}{4}, \quad a_4 = \frac{208}{45}, \quad a_5 = \frac{2425}{216}, \quad a_6 = \frac{2207}{70},$$
$$a_7 = \frac{1303841}{12960}, \quad a_8 = \frac{3059488}{8505}, \quad a_9 = \frac{7981101}{5600}, \quad a_{10} = \frac{927828775}{149688}. \tag{31}$$

Furthermore, we note numerically that

$$\frac{a_{n+2}}{a_{n+1}} - \frac{a_{n+1}}{a_n} \to C \equiv \frac{1}{r} = 0.3917 \tag{32}$$

when $n \to \infty$. To show this, we display in Fig. 1 the behavior of the sequence $\frac{a_{n+2}}{a_{n+1}} - \frac{a_{n+1}}{a_n}$ for n from 1 to 198. The consecutive differences stabilize at about 10^{-3} around $n = 10$, and at about 10^{-6} around $n = 100$. The speed of convergence is around $\frac{1}{n^2}$. Asymptotically, the asymptotic moment sequence a_n is seen to approach

$$a_n \to 2(0.39174)^n nn!, \tag{33}$$

as illustrated in Fig. 2. In the next section, we will show that the value of $C = 0.3917$ in Eq. (32) is fixed by the radius of convergence of the Taylor series for the moment sequence a_n.

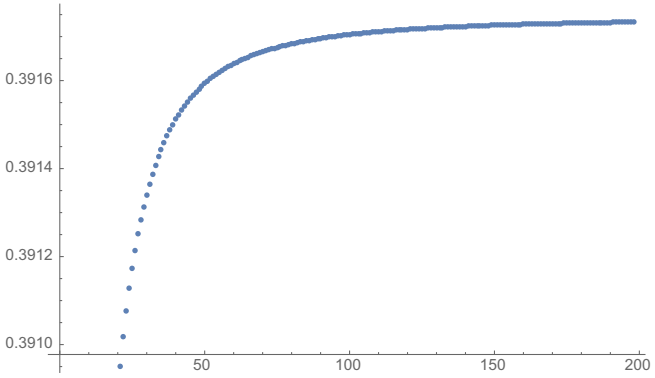

FIG. 1. Behavior of the sequences $\frac{a_{n+2}}{a_{n+1}} - \frac{a_{n+1}}{a_n}$ for $1 \le n \le 198$.

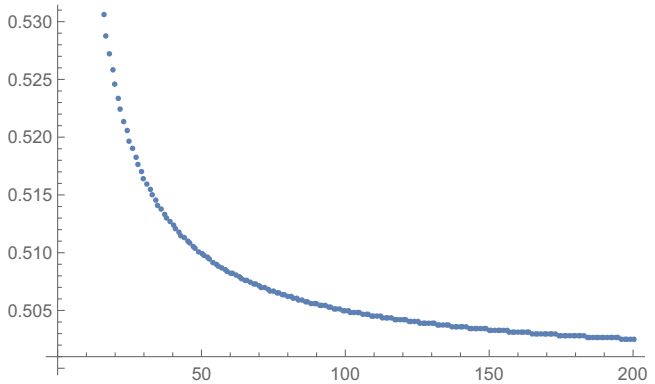

FIG. 2. Behavior of the sequence ratio $\frac{(0.39174)^n(n+1)!}{a_n}$ for $1 \le n \le 200$.

C. KNO scaling

In this subsection, we show that for large mean multiplicity $\bar{n}$, the distribution converges to a continuum limit as

$$p_n = \frac{1}{\bar{n}} f\left(\frac{n}{\bar{n}}\right), \tag{34}$$

with a universal probability distribution function or scaling function $f(z)$. To show this, one introduces the rescaled dipole number $\hat{n} = \frac{n}{\bar{n}}$. The result in the previous subsection implies that in the large-rapidity limit, one has for each k

$$\lim_{\rho\to\infty} \left\langle \hat{n}\left(\hat{n} - \frac{1}{\bar{n}}\right)\ldots\left(\hat{n} - \frac{k-1}{\bar{n}}\right)\right\rangle = a_k, \tag{35}$$

where the expectation $\langle\ldots\rangle$ is defined in terms of the dipole probability distribution p_n in Eq. (4) and a_k is the asymptotic moment sequence defined in Eq (25). Since $\frac{1}{\bar{n}} \to e^{-2\sqrt{\rho}} \to 0$ in the large-ρ limit, the above implies that the standard kth moment of $\hat{n}$ converges to the asymptotic moment sequence a_k as well:

$$\lim_{\rho\to\infty} \langle \hat{n}^k \rangle = a_k. \tag{36}$$

Based on the method of moments, which states that convergence in moments implies convergence in distribution,[4] Eq. (36) implies that $\hat{n}$ converges in the large-ρ limit *in distribution* to a random variable z with the probability distribution function $f(z)$, such that the a_k is nothing but its moment sequence:

$$\hat{n} = \frac{n}{\bar{n}}\bigg|_{\rho\to\infty} \to z, \qquad \lim_{\rho\to\infty} \langle \chi_{\hat{n}\in A} \rangle = P[z \in A] = \int_A f(z)dz, \tag{37}$$

$$a_k = \int_0^\infty dz z^k f(z). \tag{38}$$

In the above, $\chi_{\hat{n}\in A}$ is the characteristic function of the event $\hat{n} \in A$, and the expectation value $\langle\ldots\rangle$ is still defined with

[4]The condition of the method of moments—namely, that the limiting sequence a_k is a moment sequence that uniquely determines the underlying probability distribution—is indeed satisfied in this case.

respect to p_n. On the other hand, $P[z \in A]$ is the probability of finding z in the set A, according to the probability distribution $f(z)$. It is easy to see that Eq. (37) is nothing but an academic way (or "rigorous" way) to express the KNO scaling relation in Eq. (34).

As a result, the task reduces to finding a probability distribution $f(z)$, with a_n being its moment sequence. The asymptotics $a_n \to 2(0.39174)^n n(n)!$ grows quickly and satisfies the Carleman condition, implying that the resulting $f(z)$ is unique. Unfortunately, reconstructing $f(z)$ directly from a_n is a hard inverse problem in general. However, the large-k asymptotics of a_k already suggests that for large z, the distribution decays like

$$f(z)|_{z\to\infty} \to 2r^2 z e^{-zr}. \tag{39}$$

This will be confirmed by different arguments in the following section.

III. THE KNO SCALING FUNCTION

Generally, reconstructing a probability distribution from its moment sequence is a hard inverse problem. However, in the current case, since the asymptotic moment sequence a_n is inherited from a second-order differential equation in the large-ρ limit, we expect that its exponential generating function $Z(t)$,

$$Z(t = -e^u) = \sum_{n=0}^{\infty} \frac{a_n}{n!} e^{nu}, \tag{40}$$

also satisfies a second-order differential equation. Indeed, if one introduces

$$W = \ln Z, \tag{41}$$

then it is not hard to show using Eqs. (27) and (28) that W obeys a simpler equation,[5]

$$\frac{d^2}{du^2} W(u) = e^{W(u)} - 1, \tag{42}$$

with the boundary condition that for $u \to -\infty$, $W \to e^u$. Equation (42) can then be integrated readily, and analytically continued to the whole complex plane to obtain the Fourier-Laplace transform of the scaling function f:

$$Z(t) = \mathcal{L}(f)(t) = \int_0^{\infty} e^{-tz} f(z) dz. \tag{43}$$

The complex analytic Fourier-Laplace transform automatically includes the standard Fourier transform of f at $t = i\mathcal{R}$, or $u = \mathcal{R} \pm \frac{\pi}{2} i$, from which $f(z)$ can be finally obtained by taking the inverse Fourier transform. We should emphasize that the complex analytic methods are crucial to obtaining the Fourier transform of $f(z)$, since its Taylor expansion in terms of the moments,

$$Z(it) = \sum_{n=0}^{\infty} \frac{a_n}{n!} (-1)^n (it)^n, \tag{44}$$

has a finite radius of convergence $r = \frac{1}{C}$.

A. Integral representation of W

To proceed, we first notice that Eq. (42) can be integrated as [56,57]

$$u = c + \int_1^W \frac{dU}{\sqrt{2e^U - 2U - 2}}, \tag{45}$$

where the constant c can be fixed by imposing the boundary condition $W|_{u\to-\infty} \to e^u$ as

$$c = -\int_1^0 dU \left(\frac{1}{\sqrt{2e^U - 2U - 2}} - \frac{1}{U} \right). \tag{46}$$

Therefore, we obtain the integral representation of W:

$$u = \int_0^1 dU \left(\frac{1}{\sqrt{2e^U - 2U - 2}} - \frac{1}{U} \right) + \int_1^{W(u)} \frac{dU}{\sqrt{2e^U - 2U - 2}}. \tag{47}$$

The integral is along the real axis from 1 to $W(u)$. This completely determines $W(u)$ for $-\infty < u < \ln r$, where as $u \to \ln r^-$ from the lower side, W diverges to positive infinity. This corresponds to nothing but the radius of convergence $r = 1/C$ for the series representation [Eq. (44)],

$$\ln r = \int_0^1 dU \left(\frac{1}{\sqrt{2e^U - 2U - 2}} - \frac{1}{U} \right) + \int_1^{\infty} \frac{dU}{\sqrt{2e^U - 2U - 2}} = 0.93715, \tag{48}$$

with

$$C = \frac{1}{r} = e^{-0.93713} = 0.391743. \tag{49}$$

This value of C is in good agreement with the numerical observation in Eq. (32), since the convergence radius is always inverse to the rate of the exponential part for a_n when $n \to \infty$.

Furthermore, the behavior of W when $u \to \ln r^-$ can be worked out from the equation

[5] An equivalent equation has been obtained before for jet multiplicities [56,57].

$$\int_W^\infty \frac{dU}{\sqrt{2e^U - 2U - 2}} = \ln r - u, \tag{50}$$

which, after expanding the square root around the dominant term $2e^U$, reads

$$\sqrt{2}e^{-\frac{W}{2}} + \frac{1}{3\sqrt{2}} e^{-\frac{3}{2}W}\left(W + \frac{5}{3}\right) + \mathcal{O}\left(W^2 e^{-\frac{5}{2}W}\right) = \ln r - u. \tag{51}$$

To solve it, we split $W = W_0 + W_1$ with

$$e^{-\frac{W_0}{2}} = \frac{\ln r - u}{\sqrt{2}},$$
$$e^{-\frac{W_1}{2}} = 1 - \frac{(\ln r - u)^2}{12}\left(-2\ln\frac{\ln r - u}{\sqrt{2}} + \frac{5}{3}\right), \tag{52}$$

which implies for Z the following:

$$Z(u) = \frac{2}{(\ln r - u)^2} + \frac{1}{3}\left(-2\ln\frac{\ln r - u}{\sqrt{2}} + \frac{5}{3}\right) + \mathcal{O}(\ln r - u). \tag{53}$$

Therefore, Z has a double "pole" around the singularity, which exactly implies that $f(z) \sim 2r^2 z e^{-rz}$ at large z. Moreover, the coefficient 2 matches precisely the 2 in the asymptotic form of a_k. This has to be compared to the $0+1$ reduction case, where one has the equation

$$u = \int_0^1 dU\left(\frac{1}{e^U - 1} - \frac{1}{U}\right) + \int_1^{W(u)} \frac{dU}{e^U - 1}, \tag{54}$$

and as $u \to 0$,

$$Z(u) \sim -\frac{1}{u}, \tag{55}$$

which implies that Z has only a single pole.

B. Analyticity structure of Z

We have already obtained the $W(t)$ in the region $-r < t < 0$. It is time to extend it to the whole complex plane. For this, we need to understand the singularity structure of the integrand

$$G(w) = \frac{1}{\sqrt{2e^w - 2w - 2}}. \tag{56}$$

The entire function $g(w) = 2e^w - 2w - 2$ has a double pole at $w = 0$, and infinitely many nonzero single poles w_n and $\bar{w}_n$. It admits the infinite product expansion

$$2e^w - 2w - 2 = w^2 e^{\frac{w}{3}} \prod_{n=1}^\infty \frac{(w - w_n)(w - \bar{w}_n)}{|w_n|^2} e^{\frac{w}{w_n} + \frac{w}{\bar{w}_n}}. \tag{57}$$

One can show that all the nonzero poles are in the right half-plane, and the first root occurs at $w_1 = 2.088 + 7.46149i$, $\bar{w}_1 = 2.088\text{–}7.46149i$. For large n, we have $w_n \to \ln(2n + \frac{1}{2})\pi + (2n + \frac{1}{2})\pi i$. In fact, by expanding around $w = (2n + \frac{1}{2})\pi i \equiv A_n i$, one obtains an approximate formula for the location of the poles:

$$w_n = x_n + iy_n,$$
$$x_n = \ln A_n + \frac{\ln^2 A_n - 1}{2A_n^2} + \mathcal{O}\left(\frac{\ln^4 A_n}{A_n^4}\right),$$
$$y_n = A_n - \frac{1 + \ln A_n}{A_n} + \mathcal{O}\left(\frac{\ln^3 A_n}{A_n^3}\right). \tag{58}$$

This approximation is better than expected, as the first pole is already reproduced within three digits of accuracy. Given the poles, we define $G(w)$ as

$$G(w) = \frac{1}{w} e^{-\frac{w}{6}} \prod_{n=1}^\infty \frac{-|w_n|}{(w - w_n)^{\frac{1}{2}}(w - \bar{w}_n)^{1/2}} e^{-\frac{w}{2w_n} - \frac{w}{2\bar{w}_n}}. \tag{59}$$

The square roots are defined with branch cuts extending from w_n to $w_n + \infty$, and $\bar{w}_n$ to $\bar{w}_n + \infty$; namely, for w_n, the arguments go from 0 to 2π, and the same for $\bar{w}_n$. The minus sign in the numerator will guarantee that $G(w)$ is positive along the positive real axis, while it is negative along the negative real axis. Therefore, $G(w)$ is analytic in the left half-plane $\mathrm{Re}(w) < 0$ and has a single pole at $w = 0$. In the right half-plane, it has infinitely many branch cuts extending to positive infinity.

Given the knowledge of $G(w)$ and its singularity structure, one can determine $Z(t)$ for t outside the initial region $-r < t < 0$ by specifying the integration paths (in fact, the end point) for W. We first demonstrate this for $-\infty < t < -r$. One first notices that for $u \to \ln r^+$ or $t \to -r^-$, W must approach $\infty \pm 2\pi i$. In fact, the real and imaginary parts for W when u is still real must satisfy

$$\int_{\mathrm{Re}(W) - i\mathrm{Im}(W)}^{\mathrm{Re}(W) + i\mathrm{Im}(W)} dw G(w) = 0. \tag{60}$$

Therefore, we need to show that asymptotically $\mathrm{Im}(W) \to 2\pi$, as $\mathrm{Re}(W) \to +\infty$. Indeed, this is the case, since for very large $\mathrm{Re}(W)$, we have

$$\int_{\mathrm{Re}(W) - i\mathrm{Im}(W)}^{\mathrm{Re}(W) + i\mathrm{Im}(W)} dw G(w) \sim \int_{\mathrm{Re}(W) - i\mathrm{Im}(W)}^{\mathrm{Re}(W) + i\mathrm{Im}(W)} dw e^{-w/2}, \tag{61}$$

for which $\mathrm{Im}(W) \to 2\pi$ is justified. When the condition in Eq. (60) is satisfied, u as given by Eq. (47), is real and larger than $\ln r$. Furthermore, when u increases, the real part of W decreases, and one can show that $\mathrm{Im}W$ has to increase. However, the path will never meet the branch cuts for $G(z)$,

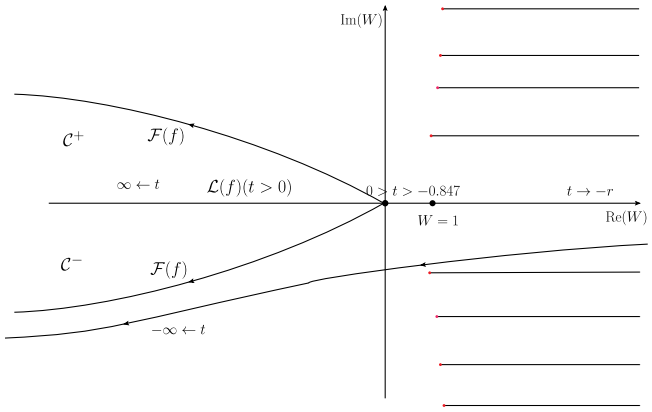

FIG. 3. We display different regions for the analytic continuation for W. Explicitly shown are the trajectories for end points of $W(t)$ in Eq. (47), whereas the integration path is from $U=1$ to W without touching singularities. The branch cuts are shown as horizontal lines. The labels $\mathcal{F}(f)$, $\mathcal{L}(f)$ denote the Fourier and Laplace transforms of the underlying probability distribution f. In particular, for $t>0$, the end point W must be located at the negative real axis, while the path runs from $U=1$ to $U=-|W|$ along the real axis, with the pole at $U=0$ circumvented through a small circle in the upper or lower half-plane, which gives rise to the imaginary part $\pm i\pi$ for u. On the other hand, to get the Fourier transform, u must have an imaginary part, $\pm\frac{i\pi}{2}$. For this, the end point W must be located along the curve $\mathcal{F}(f)$, while the integration path runs first from $U=+1$ to $U=-|\mathrm{Re}W|$ along the real axis as before, and then vertically to $\mathrm{Im}W$. In particular, the $\frac{\pi i}{2}$ goes into the upper half-plane, and the $-\frac{\pi i}{2}$ goes into the lower half-plane. The region $\mathcal{C}^+$ and $\mathcal{C}^-$ between the Laplace transform and the Fourier transform is the usual analyticity region for the characteristic function of a positively supported probability distribution.

and as $t\to-\infty$ or $u\to+\infty$, $\mathrm{Re}(W)$ approaches $-\infty$ along the curve depicted in Fig. 3.

Similarly, the integration paths for the Fourier transform $\mathcal{F}(f)$, corresponding to $\mathrm{Im}(u)=\pm\frac{\pi}{2}$, and the Laplace transform with $t>0$, corresponding to $\mathrm{Im}(u)=\pm\pi$, can be worked out. The results are shown in Fig. 3. In particular, the pole of $G(w)$ at $w=0$ contributes to the desired imaginary part $\pm i\pi$ in the case of the Laplace transform when the end point W for the integration path moves from the positive to negative axis. Similarly, the aggregation of the imaginary parts $\pm i\pi$ due to the pole and another $\mp i\frac{\pi}{2}$ acquired in the vertical path when U goes from $(\mathrm{Re}(W),0)$ to $(\mathrm{Re}(W),\mathrm{Im}(W))$ contributes to the total $\pm i\frac{\pi}{2}$ in the case for the Fourier transform. The analyticity structure for the Fourier-Laplace transform is summarized in Fig. 4. There is clearly a one-to-one correspondence between Figs. 3 and 4.

C. Asymptotics of the KNO scaling function

Given the analytic Fourier-Laplace transform, the behavior of the scaling function $f(z)$ follows readily. In fact, the

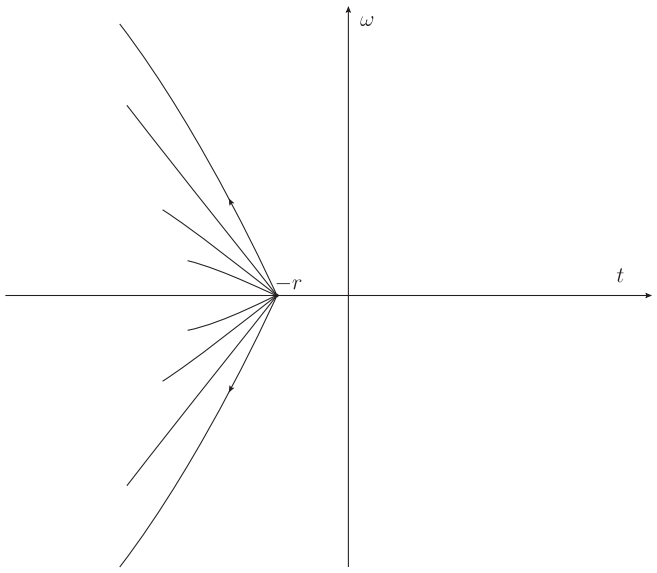

FIG. 4. The analyticity structure of the Fourier-Laplace transform of f. The Laplace transform corresponds to the positive real axis, while the Fourier transform corresponds to the imaginary axis. The singularity at $t=-r$ controls the large-z behavior of the probability distribution, and it is the source of infinitely many branch cuts corresponding to the roots. The outer ones shown with arrows correspond to w_1 and $\bar{w}_1$.

asymptotics of $f(z)$ for large z is closely related to the behavior of $Z(t)$ around $t=-r$, while the small-z behavior of $f(z)$ can be deduced from the large $\mathrm{Re}(t)\to+\infty$ asymptotics for $Z(t)$. We discuss them separately.

1. Small-z behavior

To determine the decay rate at small z, one needs to work out the behavior for $\mathcal{L}(f)(t)$ at large t or $\mathcal{F}(f)(\omega)$ at large ω. It is sufficient to consider the Laplace transform. Clearly, for $t\to\infty$, $\mathrm{Re}(W)$ must go to $-\infty$. More precisely, the Laplace transform is determined by the representation

$$\ln t=\int_{-1}^{0}dU\left(\frac{1}{\sqrt{2e^U-2U-2}}+\frac{1}{U}\right)+\int_{W(t)}^{-1}\frac{dU}{\sqrt{2e^U-2U-2}},\tag{62}$$

which will guarantee that for $t\to0^+$, one has the correct boundary condition:

$$W(t)\to-t.\tag{63}$$

For large $|W|$, we can expand

$$\int_1^{|W|}\frac{dU}{\sqrt{2U-2+2e^{-U}}} = \int_1^{|W|}\frac{dU}{\sqrt{2U-2}}+\int_1^{|W|}\left(\frac{1}{\sqrt{2U-2+2e^{-U}}}-\frac{1}{\sqrt{2U-2}}\right). \tag{64}$$

Now, for large $|W|$, the last integral is convergent, so that for $t\to\infty$,

$$\ln t = \int_{-1}^{0} dU\left(\frac{1}{\sqrt{2e^U-2U-2}}+\frac{1}{U}\right) + \int_1^{\infty}\left(\frac{1}{\sqrt{2U-2+2e^{-U}}}-\frac{1}{\sqrt{2U-2}}\right) + \sqrt{-2W-2}, \tag{65}$$

or

$$\ln t + 0.411926 = \sqrt{-2W-2}, \quad \to \quad W = -1-\frac{1}{2}\ln^2(\alpha t)+\mathcal{O}\left(e^{-\frac{1}{2}\ln^2(\alpha t)}\right), \tag{66}$$

which implies that for large t,

$$\mathcal{L}(f)(t)\to\exp\left[-1-\frac{1}{2}\ln^2(\alpha t)\right], \tag{67}$$

where $\alpha = 1.50972$ is a pure number. It is not hard to show that the above gives the correct asymptotics for $Z(t)$ with $\mathrm{Re}(t)\to+\infty$.

Given the above, at small z, one can simply shift the contour of inverse Fourier transform to $\frac{1}{z}+it$ in order to reach the asymptotic region. After simple algebra, one has

$$f(z) = \frac{1}{2\pi z}\exp\left(-\frac{1}{2}\ln^2\frac{\alpha}{z}\right)\int_{-\infty}^{\infty}dt \times\exp\left[-\ln\frac{\alpha}{z}\ln(1+it)+it-\frac{1}{2}\ln^2(1+it)\right]. \tag{68}$$

One must now determine the asymptotics of the integral at small z. Applying the saddle-point analysis, one finally has

$$f(z) = \frac{1}{z}\ln\frac{\alpha}{z}\exp\left(-\frac{1}{2}\ln^2\frac{\alpha}{z}-\ln\frac{\alpha}{z}\ln\ln\frac{\alpha}{z}+\ln\frac{\alpha}{z} -\frac{1}{2}\ln^2\ln\frac{\alpha}{z}-2+\mathcal{O}\left(\frac{\ln^2\ln\frac{\alpha}{z}}{\ln\frac{\alpha}{z}}\right)\right). \tag{69}$$

The speed of growth is much slower than the $0+1$D reduction, but much faster than the $1+2$D case.

2. Large-z behavior

To determine the large-z behavior, we now use the Fourier inverse transform,

$$f(z) = -i\int_{-i\infty}^{i\infty}\frac{dt}{2\pi}e^{tz}Z(t). \tag{70}$$

For large z, one would like to shift the integration path as far left as possible. The singularity at $t=-r$ will prevent shifting the contour further and gives rise to the leading exponential decay. The singular part of Z near $t=-r$ along the real axis has already been given in Eq. (53) in terms of $u=\ln(-t)$. Expressed in terms of t, it reads

$$Z(t)|_{t\to -r} = \frac{2r^2}{(t+r)^2}-\frac{2r}{t+r}+\frac{1}{3}\left(-2\ln\frac{t+r}{\sqrt{2r}}+\frac{13}{6}\right) + \mathcal{O}((t+r)\ln(t+r)). \tag{71}$$

The above applies to all the directions $t+r=|t+r|e^{i\theta}$ when $|\theta|\le\frac{\pi}{2}$, including the vertical line $t=-r+ix$:

$$Z(-r+ix)|_{x\to 0} = -\frac{2r^2}{x^2}-\frac{2r}{ix}+\frac{1}{3}\left(-2\ln\frac{ix}{\sqrt{2r}}+\frac{13}{6}\right) + \mathcal{O}(x\ln(x)). \tag{72}$$

Now, shifting the contour with a small circle centered at $t=-r$, we have

$$f(z)e^{rz} = \int_{-\infty}^{-\epsilon}\frac{dx}{2\pi}e^{ixz}Z(-r+ix)+\int_{\epsilon}^{\infty}\frac{dx}{2\pi}e^{ixz}Z(-r+ix) + \int_{C_\epsilon}\frac{dx}{2\pi}e^{ixz}Z(-r+ix). \tag{73}$$

Using the explicit form of the singularity for $Z(-r+ix)$ for small x, and the fact that $Z(-r+ix)$ decays as $e^{-\frac{\ln^2 ix}{2}}$ for large ix, and is infinitely smooth when $x\neq 0$, we obtain

$$f(z) = 2r\left(rz-1+\mathcal{O}\left(\frac{\ln z}{z}\right)\right)e^{-rz}, \qquad z\to\infty. \tag{74}$$

Equations (69) and (74) are the major results of this section.

IV. DLA KNO SCALING VERSUS H1 DATA

Although the asymptotics of the DLA for $f(z)$ can be obtained exactly as presented in the previous section, the full shape of $f(z)$ can only be obtained numerically, with the help of the inverse Fourier transform. For that, we choose to invert with the complex valued path

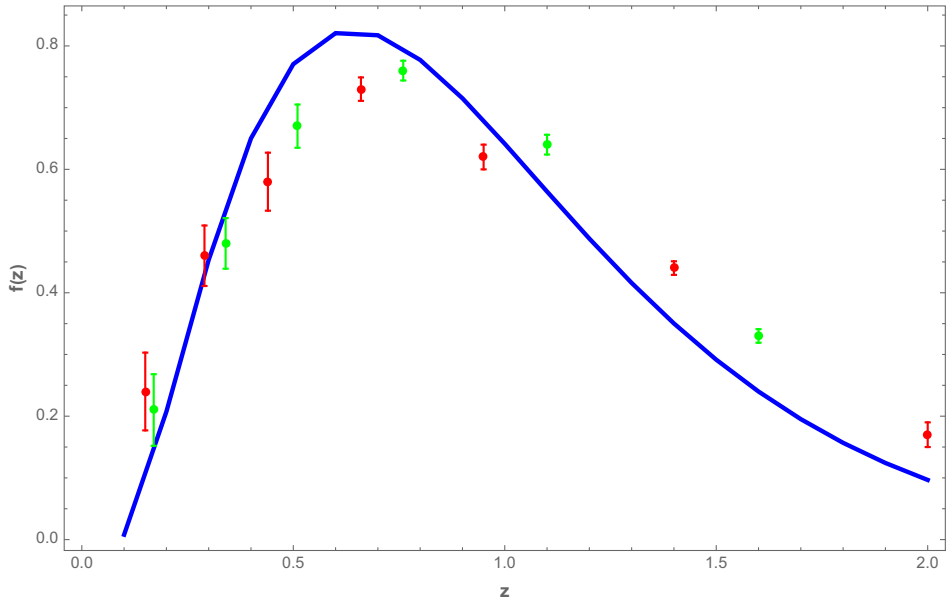

FIG. 5. The exact scaling of the KNO particle multiplicity $f(z)$ as in Eq. (76) with a peak around $z = 0.6$, following from the DLA of Mueller's dipole wave function evolution (solid blue curve). The data is the measured KNO scaling function $\Psi(z)$ for the charged particle multiplicities in ep DIS scattering, as reported by the H1 Collaboration in Ref. [28], for $\sqrt{s} = 319$ GeV, photon virtualities $40 < Q^2 < 100$ GeV^2, and charged particle pseudorapidities in the range $0 < \eta < 4$, for two different inelasticities: $0.15 < y_I < 0.3$ (green) and $0.3 < y_I < 0.6$ (red) [28].

$$\mathcal{C}_\gamma = -x \pm \gamma\pi\sqrt{2x}i, \qquad 0 < x < \infty, \tag{75}$$

in terms of which the inverse Fourier transform reads

$$f(z) = -\frac{i}{2\pi}\int_{\mathcal{C}_\gamma} \frac{WdW}{\sqrt{2e^W - 2W - 2}} \exp[g(W) + W - zWe^{g(W)}],$$
$$g(W) = \int_W^0 dU \left(\frac{1}{\sqrt{2e^U - 2U - 2}} + \frac{1}{U}\right). \tag{76}$$

This choice of the path guarantees that the integrand decays exponentially for large x, for the parameter γ in the range $\frac{1}{\sqrt{2}} \leq \gamma \leq 2$. In fact, the natural path for the Fourier transform asymptotically approaches $\mathcal{C}_{\frac{1}{\sqrt{2}}}$. Clearly, the result is path independent, provided that the path ensures convergence at infinity. For convenience, the numerical values of $f(z)$ in the nonasymptotic regime are tabulated in Table I.

TABLE I. Table of the scaling function.

z	$f(z)$	z	$f(z)$
0.1	0.01	1.1	0.56
0.2	0.21	1.2	0.49
0.3	0.45	1.3	0.42
0.4	0.65	1.4	0.35
0.5	0.77	1.5	0.29
0.6	0.82	1.6	0.24
0.7	0.82	1.7	0.20
0.8	0.78	1.8	0.16
0.9	0.72	1.9	0.12
1.0	0.64	2.0	0.1

In Fig. 5, we show in solid blue the numerical result for $f(z)$ [Eq. (76)] in the range $0.1 < z < 2$, with a peak around $z = 0.6$. The result for the DLA $f(z)$ compares well to the measured KNO scaling function $\Psi(z)$ for the charged particle multiplicities, reported by the H1 Collaboration [28]. The charged multiplicities are measured in ep DIS scattering, for $\sqrt{s} = 319$ GeV, photon virtualities $40 < Q^2 < 100$ GeV^2, and charged particle pseudorapidities in the range $0 < \eta < 4$, for two different inelasticities: $0.15 < y_I < 0.3$ (green) and $0.3 < y_I < 0.6$ (red). In Fig. 6, we compare the KNO scaling function in the diffusive regime e^{-z} (solid black) to the exact DLA asymptotics [Eq. (74)] (solid blue). The DIS data at HERA support the DLA solution we have presented for the entire range of z, over the diffusive solution.

V. RELATION TO JET EVOLUTION

As we mentioned in our introductory remarks, the DLA scaling function for Mueller's dipole evolution is identical to that of jet evolution [56,57].[6] This is not accidental, and it follows from the correspondence with the BK-BMS evolution equation [58–62], as we now detail. When limited to the virtual part only, this correspondence is also called "soft rapidity" correspondence [64]. We will provide a

[6]This equality has been briefly pointed out in Ref. [65].

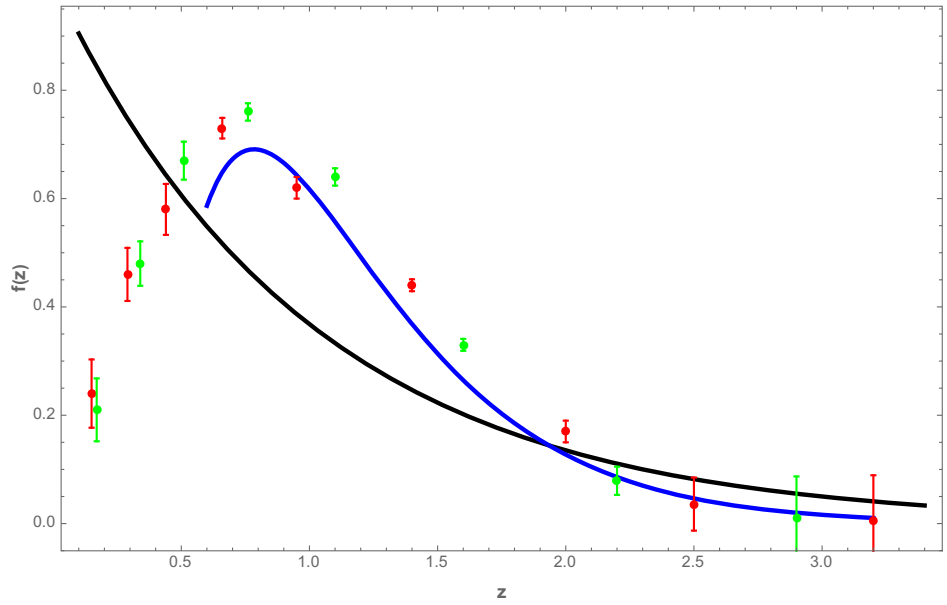

FIG. 6. The exact asymptotic scaling of the KNO particle multiplicity $f(z)$ as in Eq. (74), following from the DLA of Mueller's dipole wave function evolution (solid blue curve). For comparison, we show the KNO particle multiplicity e^{-z}, following from the $0+1$D reduction or diffusive approximation of Mueller's dipole wave function evolution (solid black curve). The data are from the H1 Collaboration in Ref. [28].

pedagogical introduction to this correspondence at leading order, using the generating functional approach in Ref. [8] by emphasizing the underlying time and energy ordering of the soft gluon emission. In particular, we will show that the double logarithm limit in the BMS equation has the same angular ordering as that in Refs. [56,57], which maps to the dipole size ordering of the dipole evolution under the conformal transformation discussed in Refs. [63,64]. As a result, the two scaling functions are identical.

A. Generating function approach to BMS equation

The BMS equation, describing the "nonglobal" logarithms in the e^+e^- annihilation process, is based on the universal feature of the underlying branching process, where a large number of soft gluons is released as asymptotic final states, with infrared divergent contributions to the total cross section. In the eikonal approximation, which is sufficient for our purpose, the energetic quark-antiquark pairs are represented by a Wilson-line cusp consisting of lightlike gauge links with direction 4-vectors $p=(1,\vec{p})$ and $n=(1,\vec{n})$:

$$\mathcal{W}_{np}=\mathcal{T}\left(\mathcal{P}e^{ig\int_0^\infty ds p\cdot A(ps)}\mathcal{P}e^{ig\int_\infty^0 ds n\cdot A(ns)}\right). \quad (77)$$

The amplitudes consisting of n soft gluons with momenta $k_1,\ldots k_n$ emitted from the Wilson-line cusp $\mathcal{W}_{np}$ as final states, read

$$\langle k_1,\ldots k_n|\mathcal{W}_{np}|\Omega\rangle = iM_n(k_1,k_2,\ldots k_n). \quad (78)$$

The n-gluon contribution to the total cross section,

$$\sigma_n=\frac{1}{n!}\int d\Gamma_1 d\Gamma_2\ldots d\Gamma_n|M_n(k_1,k_2,\ldots k_n)|^2, \quad (79)$$

normalizes to 1, thanks to unitarity:

$$\sum_{n=0}^{\infty}\sigma_n=1. \quad (80)$$

However, there are logarithmic IR divergences in σ_n, represented as logarithms formed between the UV cutoff E and the IR cutoff $E_0\gg\Lambda_{\rm QCD}$. We are interested in the "most singular" part of σ_n—namely, the part in which a logarithm $\ln\frac{E}{E_0}$ always comes with α_s. It turns out that this part of the σ_n can be effectively generated through a simple Markov process. More precisely,

(1) In time-order perturbation theory, the emitted soft gluons are strongly ordered in energies: $E\gg\omega_1\gg\omega_2\gg\cdots\omega_n\gg E_0$.
(2) Softer gluons are emitted later in time; harder gluons are emitted earlier in time.
(3) Each time a softer gluon with momentum k is emitted from a harder gluon with momentum p, a factor $\frac{qp^\mu}{p\cdot k}$ for the emission kernel follows, in the eikonal approximation.

It is easy to check that for emission processes violating one or more of the above properties, such as a softer gluon emitted first, the contribution to σ_n will be less singular.

For an illustration of the energy and time ordering, see Figs. 7 and 8.

We first consider the two-gluon diagram in Fig. 7. In covariant perturbation theory, the diagram is proportional to

$$\text{Fig. 7} = -\frac{1}{2}C_A C_F \int \frac{d^2\Omega_1 d^2\Omega_2}{(2\pi)^4} \int \frac{\omega_1^2\omega_2^2 d\omega_1 d\omega_2}{4\omega_1\omega_2(2\pi)^2} \frac{g^4}{(k_1+k_2)\cdot p k_2\cdot p (k_1+k_2)\cdot n} \times \frac{-(2k_1+k_2)^\mu n^\nu + (2k_2+k_1)^\nu n^\mu + (k_1-k_2)\cdot n g^{\mu\nu}}{(k_1+k_2)^2} p_\mu p_\nu, \tag{81}$$

where the color factor comes from $if^{abc}t^a t^b t^c = \frac{i}{2}f^{abc}[t^a,t^b]t^c = -\frac{C_A C_F}{2}$. Now, consider the region $|\vec{k}_1| \gg |\vec{k}_2|$; in this case, the triple-gluon vertex simplifies to $-2k_1^\mu n^\nu + k_1^\nu n^\mu + k_1\cdot n g^{\mu\nu}$. The last term vanishes due to $p^2 = 0$. The second term proportional to k_1^ν (longitudinal) will cancel with contributions from polarization diagrams after using Ward identities, leaving only the physically motivated eikonal current $\frac{2k_1^\mu n^\nu}{2k_1\cdot k_2}$. As a result, the contribution in this region in the $C_F \sim \frac{N_c}{2}$ (large color) limit, is

$$\text{Fig. 7}|_{\omega_1\gg\omega_2} = \left(\frac{\alpha_s N_c}{2\pi}\right)\int\frac{d\omega_1}{\omega_1}\int\frac{d\Omega_1}{4\pi}\frac{p\cdot n}{\hat{k}_1\cdot p\hat{k}_1\cdot n}\left(\frac{\alpha_s N_c}{2\pi}\right) \times \int\frac{d\omega_2}{\omega_2}\int\frac{d\Omega_2}{4\pi}\frac{\hat{k}_1\cdot p}{\hat{k}_2\cdot\hat{k}_1\hat{k}_2\cdot p}, \tag{82}$$

with the desired factorized form, producing the leading logarithm. On the other hand, in the region $\omega_2 \ll \omega_1$, it is clear that the energy integral is

$$\text{Fig. 7}|_{\omega_2\gg\omega_1} \propto \int\frac{\omega_2^2 d\omega_2}{2\omega_2\times\omega_2^4}\times\omega_2\int\frac{\omega_1^2 d\omega_1}{2\omega_1\times\omega_1} = \int\frac{d\omega_2}{4\omega_2^2}\int d\omega_1 = \int\frac{d\omega_2}{4\omega_2}, \tag{83}$$

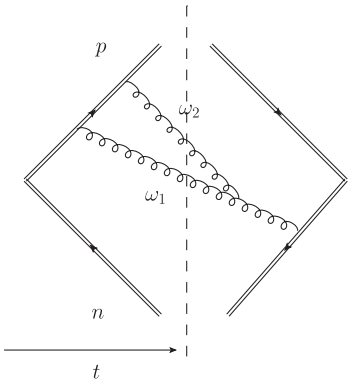

FIG. 7. A sample diagram with two real gluons. The direction of time is shown as an arrow for the amplitudes (left of the cut), and the opposite for the conjugate amplitudes (right of the cut). The region $\omega_1 \gg \omega_2$ contributes to the leading logarithm $\alpha_s^2 \ln^2\frac{E}{E_0}$ for σ_2.

which only leads to a single logarithm. It is easy to check that in the time-ordered perturbation theory, the energy denominators are in one-to-one correspondence with the eikonal propagators. For example, in the region $\omega_1 \gg \omega_2$, we have for the time order shown in Fig. 7

$$\frac{1}{\omega_1+\omega_2-\vec{p}\cdot(\overrightarrow{k_1}+\overrightarrow{k_2})}\frac{1}{\omega_2-\vec{p}\cdot\overrightarrow{k_2}}\frac{1}{\omega_1+\omega_2-|\overrightarrow{k_1}+\overrightarrow{k_2}|} \times\frac{1}{\omega_1+\omega_2-\vec{n}\cdot(\overrightarrow{k_1}+\overrightarrow{k_2})} \sim \frac{1}{k_1\cdot p}\frac{1}{k_2\cdot p}\frac{1}{k_2\cdot\hat{k}_1}\frac{1}{k_1\cdot n}. \tag{84}$$

The contribution for another time ordering with a backward-moving gluon on the conjugate amplitude side is suppressed by more $(\frac{1}{\omega_1})$ and is therefore less singular. Similarly, for Fig. 8, one can show that in either the $\omega_1 \gg \omega_2$ or $\omega_2 \gg \omega_1$ region, there will be no leading logarithm:

$$\text{Fig. 8}|_{\omega_1\gg\omega_2} \propto \int\frac{\omega_1 d\omega_1}{\omega_1^3}\int\frac{\omega_2 d\omega_2}{\omega_2} \propto \ln\frac{E}{E_0}, \tag{85}$$

$$\text{Fig. 8}|_{\omega_2\gg\omega_1} \propto \int\frac{\omega_2 d\omega_1}{\omega_2^3}\int\frac{\omega_1 d\omega_1}{\omega_1} \propto \ln\frac{E}{E_0}. \tag{86}$$

In the first case, the time-energy ordering is violated in the conjugate amplitude side, while in the second case, the energy-time ordering is violated in the amplitude side. It is clear that the rule that softer gluons are emitted later carries

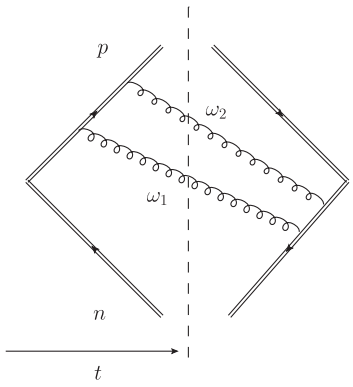

FIG. 8. Another two-gluon diagram which does not contribute to order $\alpha_s^2 \ln^2\frac{E}{E_0}$ for σ_2.

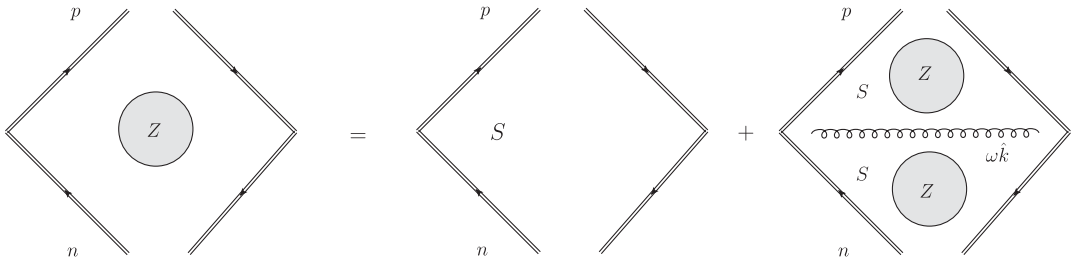

FIG. 9. Illustration of the recursive relation given in Eq. (88). S denotes the virtual Sudakov contribution. The first term after the equal sign corresponds to the pure virtual contribution to the generating function Z. The second term corresponds to the contribution with at least one real gluon—the hardest one, with momentum $k = \omega\hat{k}$, is emitted first and splits the original "dipole" into two.

to higher orders. The contribution for any leading n-gluon diagram will have a factorized form as in Eq. (82).

As a result, the emission depends only on the color charges that are already present in the final state and their energy scales, but not on the history of how they are emitted. In large N_c, the color charges effectively split the original Wilson-line cusp into many "dipoles," with the subsequent emissions to different dipoles being completely independent. To keep track of the above branching process, we follow Mueller's reasoning for the wave function evolution, and introduce the generating functional

$$\mathcal{Z}\left(\frac{E}{E_0}; n, p; \lambda\right) = \sum_{n=0}^{\infty} \lambda^n \sigma_n \tag{87}$$

for the n cross sections, which is readily seen to obey the integral equation

$$\begin{aligned}\mathcal{Z}\left(\frac{E}{E_0}; n, p; \lambda\right) &= e^{-\frac{\bar{\alpha}_s}{4\pi}\ln\frac{E}{E_0}\int d\Omega_k \frac{\hat{p}\cdot\hat{n}}{\hat{k}\cdot\hat{p}\,\hat{k}\cdot\hat{n}}} + \frac{\bar{\alpha}_s}{4\pi}\lambda \int_{E_0}^{E} \frac{d\omega}{\omega} \\ &\times e^{-\frac{\bar{\alpha}_s}{4\pi}\ln\frac{E}{\omega}\int d\Omega_k \frac{\hat{p}\cdot\hat{n}}{\hat{k}\cdot\hat{p}\,\hat{k}\cdot\hat{n}}} \int d\Omega_k \frac{\hat{p}\cdot\hat{n}}{\hat{k}\cdot\hat{p}\,\hat{k}\cdot\hat{n}} \\ &\times \mathcal{Z}\left(\frac{\omega}{E_0}; n, \hat{k}; \lambda\right)\mathcal{Z}\left(\frac{\omega}{E_0}; p, \hat{k}; \lambda\right),\end{aligned} \tag{88}$$

where $\bar{\alpha}_s = \frac{\alpha_s N_c}{\pi}$. The first term is the Sudakov contribution where all soft gluons are virtual, and the second term is the contribution where at least one soft gluon is real (we pick the hardest gluon with momentum $k = \omega\hat{k}$, which splits the Wilson-line cusp into two dipoles at energy scale ω, with or without real contributions). The prefactor is $\frac{\alpha_s N_c}{\pi}$ instead of $\frac{\alpha_s N_c}{2\pi}$, as in Eq. (82), because for each real gluon emission there are two contractions, whereas Fig. 7 shows only one contraction for each of the two gluons. See Fig. 9 for an illustration of the recursive relation [Eq. (88)]. It is easy to check that for $\lambda = 1$, one simply has $Z = 1$, the required normalization property. The above is nothing but the integral form of the BMS equation [58,60]. To cast it as a differential equation, one takes the derivative with respect to $\ln\frac{E}{E_0}$,

$$\begin{aligned}&\frac{d}{d\ln\frac{E}{E_0}}\mathcal{Z}\left(\frac{E}{E_0}; n, p; \lambda\right) \\ &= \frac{\bar{\alpha}_s}{4\pi}\int d\Omega_k \frac{\hat{p}\cdot\hat{n}}{\hat{k}\cdot\hat{p}\,\hat{k}\cdot\hat{n}}\left(-\mathcal{Z}\left(\frac{E}{E_0}; n, p; \lambda\right)\right. \\ &\left. + \lambda\mathcal{Z}\left(\frac{E}{E_0}; n, \hat{k}; \lambda\right)\mathcal{Z}\left(\frac{E}{E_0}; p, \hat{k}; \lambda\right)\right),\end{aligned} \tag{89}$$

which is the standard form of the BMS equation in Refs. [58,60].

After introducing the BMS equation, we would like to provide a few comments from a field-theoretical perspective. The "power expansion" in asymptotically free quantum field theories is distinct from that for superrenormalizable or conformal field theories, by additional logarithmic contributions that couple UV and IR scales.[7] In particular, the squared amplitudes for "asymptotic gluons" integrated over their pertinent phase space suffers from logarithmic IR divergences with an involved nonlinear pattern as in Eq. (88). When these partial contributions are used as building blocks for other quantities, sometimes miracle cancellation occurs, and the logarithms in the final result follow a much simpler linear pattern. This normally happens when the IR scale E_0 is introduced through globally conserved quantities, such as the transverse momentum $Q_\perp$. However, in many other cases, the nonlinear pattern of logarithms survives. This is the case for the original "BMS nonglobal logarithm" measuring the probability of energy flow less then E_0 outside a certain jet cone region Ω_{in} [58], which is not a conserved quantity. Another example is the total "transverse energy" $E_T = \sum_i \sqrt{\vec{k}_{i\perp}^2 + m_i^2}$, for which factorization is known to break.

B. Connecting BMS and Mueller's dipole

The generating functional approach to the BMS equation makes the connection to small-x physics very transparent. In fact, as shown by Mueller [8], small-x evolution

[7]The standard operator product expansion implies that these logarithms are controlled asymptotically by perturbation theory, as they couple to both IR and UV regimes.

TABLE II. Mueller hierarchy and BMS hierarchy.

	Dipole	Cusp
Distribution in	*Virtual* gluon in wave function	*Real* gluon in asymptotic state
Large N_c	Yes	Yes
Evolution in	Rapidity divergence	Soft divergence
Kernel	$\frac{b_{10}^2}{b_{12}^2 b_{20}^2}$	$\frac{n\cdot p}{\tilde{k}\cdot n \tilde{k}\cdot p}$
Virtual part	TMD soft factor	Sudakov form factor
Time ordering	In LF time x^+	In CM time t
Momentum ordering	Decreasing k^+	Decreasing energy ω
Virtuality ordering	Increasing	Decreasing
Markov property	Yes	Yes
DLA	$b_{10} \gg b_{12} \gg \cdots$	$\theta_{01} \gg \theta_{12} \gg \cdots$

equations such as BFKL and BK are all based on the distribution of virtual soft gluons in the light-front wave functions (LFWFs). In the famous dipole picture, based on light-front perturbation theory, it is easy to show that the leading rapidity logarithms in the norm squares of the dipole's LFWFs can be effectively generated through a very similar Markov process, where the soft gluons emitted are strongly ordered in rapidity, $x_1 \gg x_2 \cdots \gg x_n$, and gluons with larger x are emitted first. Based on this, one can write out the evolution equation for the generating function of the dipole distribution as in Sec. II.

Clearly, Eqs. (88) and (1) are very similar, in the sense that they are both generating functions for distribution of soft gluons in "final states," and both originate from a Markov branching process with the gluons strongly ordered in the evolution variables. However, there are differences. Mueller's evolution equation is for a wave function, and the evolution is towards the direction with more and more "virtuality" ($\frac{k_{1\perp}^2}{2x_1} \ll \cdots \ll \frac{k_{n\perp}^2}{2x_n}$), while in BMS the evolution is towards more and more "reality." This suggests that the mapping between the BMS and Mueller's evolutions flips the energy scale. This is only possible in the conformal limit.

Indeed, one can perform a conformal transformation to map Mueller's dipole construct, to exactly the Wilson-line cusp [63,64]. The transformation reads

$$(x^+, x^-, \vec{x}_\perp) \quad \mathcal{C}: \rightarrow \quad \left(x^+ - \frac{x_\perp^2}{2x^-}, -\frac{1}{2x^-}, \frac{\vec{x}_\perp}{\sqrt{2}x^-}\right). \tag{90}$$

It is easy to check that Eq. (90) maps a Wilson-line cusp $\mathcal{W}_{np}$ pointing to positive infinity, onto a dipole propagating along the LF time x^+ from $x^+ = -\infty$ to $x^+ = 0$:

$$\mathrm{P}\exp\left[ig\int_0^\infty dsv\cdot A(sv)\right] \quad \mathcal{C}: \rightarrow \quad \mathrm{P}\exp\left[ig\int_{-\infty}^0 dx^+ A^-\left(x^+, 0, \frac{\vec{v}_\perp}{2v^-}\right)\right]. \tag{91}$$

The asymptotic soft gluons emitted into the scattering states at $t = \infty$ become the virtual gluons present in the wave function at zero light-front time x^+. In this sense, the mapping is a "virtual-real" duality, in addition to the standard interpretation that it maps rapidity divergences to UV divergences [64].[8] Moreover, if one parametrizes the direction vector as $v = v^0(1, \vec{n})$, then the conformal transformation reduces to the standard stereographic projection, that maps $\vec{n} \in \mathrm{S}^2$ onto $\vec{b} \in \mathrm{R}^2$. See Table II for a comparison between the BMS and dipole evolution.

C. The universal DLA limit

The BK/BMS equation resums single logarithms in rapidity/energy. However, in both cases, there are two types of divergences instead of one: in Mueller's dipole, there are UV divergences (in p_n) in the large-$k_\perp$ or small-dipole region, while in the Wilson-line cusps, there are "rapidity divergences" caused by emissions collinear to the Wilson lines. It is natural to consider the double logarithms (DLs) in terms of both.[9] One can show that the leading double logarithms are generated from the same branching process, and that in addition to the strong ordering in k^+/ω, one imposes strong ordering in dipole sizes/emitting angles as well. The strong ordering in virtuality is preserved by the DL limit. Clearly, the two DL limits and the underlying size/angle orderings map onto each other under the conformal transformation [Eq. (90)]. We emphasize that the DL limit dominates the large-Q^2 limit of the e^+e^- multiplicity

[8] In nonconformal theory, the exact mapping breaks at two loops already [62]. But for the virtual part, there is a way to generalize the mapping to all orders [64].

[9] In fact, it is known that the Sudakov form factor is dominated by a double logarithm in the exponential.

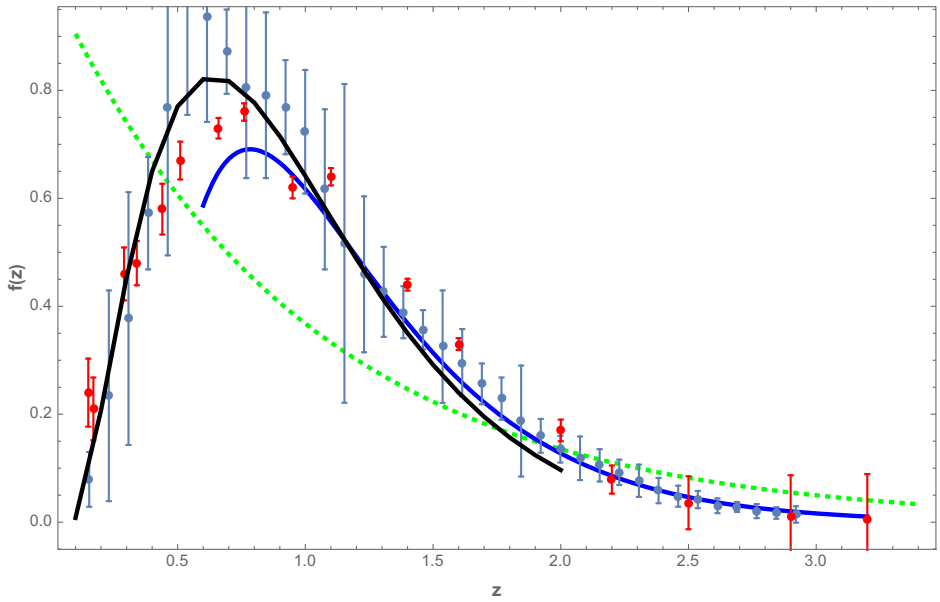

FIG. 10. The exact scaling [Eq. (76)] of the KNO particle multiplicity (solid black curve), its exact asymptotic [Eq. (74)] (solid blue curve), and the diffusive KNO multiplicity (green dashed curve), compared to the measured particle multiplicities in ep DIS scattering by the H1 Collaboration [28] (red data points), and the charged particle multiplicities from hadronic Z-decays from e^+e^- annihilation with $\sqrt{s} = 91.2$ GeV, as measured by the ALEPH Collaboration [66] (gray data points).

$$n_{e^+e^-}(Q^2) = \exp\left[2\left(\frac{N_c}{2\pi\beta_0}\ln\frac{Q^2}{\Lambda^2_{\rm QCD}}\ln\frac{\ln\frac{Q^2}{\Lambda^2_{\rm QCD}}}{\ln\frac{Q^2_0}{\Lambda^2_{\rm QCD}}}\right)^{\frac{1}{2}}\right], \tag{92}$$

while the BFKL limit [60] only contributes to

$$n_{\rm BFKL} \sim e^{\frac{N_c \ln 2}{\pi\beta_0}\ln\frac{\ln\frac{Q^2}{\Lambda^2_{\rm QCD}}}{\ln\frac{Q^2_0}{\Lambda^2_{\rm QCD}}}},$$

smaller than the DLA result in the large-Q^2 limit.

In Fig. 10, we show the exact scaling [Eq. (76)] of the KNO particle multiplicity (solid black) versus the measured multiplicities in ep DIS scattering by the H1 Collaboration [28] (red data points) and the charged particle multiplicities from hadronic Z-decays from e^+e^- annihilation with $\sqrt{s} = 91.2$ GeV, as measured by the ALEPH Collaboration [66] (gray data points). We have also shown the exact asymptotic [Eq. (74)] (solid blue) and the diffusive KNO multiplicity (dashed green) for comparison. The agreement is very good, for both datasets, underlying the universality of our results.

VI. IMPLICATION FOR THE ENTANGLEMENT ENTROPY

As we have shown in Ref. [49], the reduced density matrix measuring quantum entanglement between fast and slow degrees of freedom in Mueller's dipole wave function has the generic form

$$\rho = \sum_n p_n \rho_n, \tag{93}$$

where p_n is the total probability of finding n dipoles, and the ρ_n is an effective reduced density matrix with n soft gluons on the left and right. From Eq. (93), the entanglement entropy for ρ can be found to be

$$S = -\sum_n p_n \ln p_n + \sum_n p_n s_n, \tag{94}$$

where $s_n = -{\rm tr}\rho_n \ln\rho_n$ is the entanglement entropy of the reduced density matrix in the n-particle sector. Since the wave function peaks at $n = \bar{n}$ for large n, it is natural to expect that the entanglement entropy s_n also peaks around $n = \bar{n}$ and scales as $s(\frac{n}{\bar{n}})$. Under this assumption, the universal behavior follows

$$S = \ln\bar{n} + \int dz f(z)(-\ln f(z) + s(z)). \tag{95}$$

In particular, in the DLA regime, the use of the asymptotic form of Eq. (15) yields

$$S(\bar{n}(y,Q^2)) \to \ln(\bar{n}(y,Q^2)) \equiv 2\left(\frac{N_c}{\pi\beta_0} y \ln\frac{\ln\frac{Q^2}{\Lambda^2_{\rm QCD}}}{\ln\frac{Q^2_0}{\Lambda^2_{\rm QCD}}}\right)^{\frac{1}{2}}, \tag{96}$$

with β_0 fixed in Eq. (9). The region of validity for the DLA implies

$$y \sim \ln \frac{\ln \frac{Q^2}{\Lambda^2_{\rm QCD}}}{\ln \frac{Q_0^2}{\Lambda^2_{\rm QCD}}} \to \infty, \tag{97}$$

which shows that the largest logarithm is the double logarithm. More explicitly, Eq. (97) implies that Q^2 must be very large, putting the saturation regime out of reach in the DLA regime. The entanglement entropy [Eq. (96)] is accessible to current and future DIS measurements.

We note that although both the DLA and diffusive regimes support KNO scaling, the corresponding scaling functions are very different. In the diffusive limit, the distribution $p_n \to e^{-n/\bar{n}}$ is almost identical to the thermal distribution for a quantum oscillator with $\bar{n} \sim \frac{T}{\omega} \gg 1$, which suggests maximal decoherence encoded in the large entanglement entropy $S \sim y$. However, the multiplicity distribution in the DLA regime is far from thermal, with a much smaller entanglement entropy $S \sim \sqrt{y}$. Also, its KNO scaling function $f(z)$ carries still more structure (peak at intermediate z).

Finally, due to the similarity in the branching process underlying the BMS evolution and Mueller's dipole, one can define a reduced density matrix that entangles soft gluons in the final state at different energy scales for the leading-order BMS evolution. It satisfies a similar evolution equation that maps exactly to that for the Mueller's dipole, as we have shown in Ref. [49]. In the large-Q^2 limit, it produces a large entanglement entropy, responsible for the large observed multiplicities in jets. In the DLA limit, the entanglement entropy in jet emissivities is again given by a result similar to Eq. (96),

$$S_{\rm cusp}(\bar{n}(Q^2)) \to \ln(\bar{n}(Q^2)) \to 2\left(\frac{N_c}{2\pi\beta_0}\ln\frac{Q^2}{\Lambda^2_{\rm QCD}}\ln\frac{\ln\frac{Q^2}{\Lambda^2_{\rm QCD}}}{\ln\frac{Q_0^2}{\Lambda^2_{\rm QCD}}}\right)^{\frac{1}{2}}. \tag{98}$$

The rapidity gap between the quark-antiquark pair $y = \ln\frac{Q^2}{\Lambda^2_{\rm QCD}}$ produces another logarithm in Q^2. The argument of the square root in Eq. (98) is the Sudakov double logarithm

$$|H_{\rm suda}(Q^2)|^2 \sim e^{-\frac{N_c}{2\pi\beta_0}\ln\frac{Q^2}{\Lambda^2_{\rm QCD}}\ln\ln\frac{Q^2}{\Lambda^2_{\rm QCD}}}$$

in the large-Q^2 limit, namely

$$S_{\rm cusp}(\bar{n}(Q^2)) \to 2\sqrt{2}\left(\ln\left(\frac{1}{|H_{\rm suda}(Q^2)|}\right)\right)^{\frac{1}{2}}. \tag{99}$$

The entanglement entropy [Eq. (98)] is also accessible to currently measured emissivities from jets—say, from e^+e^- annihilation. As mentioned before, in the case of e^+e^-, the DLA dominates the large-Q^2 limits in comparison to the BFKL contribution.

VII. CONCLUSION AND OUTLOOK

We have presented an exact derivation of the leading moments of the dipole emissivities from the dipole cascade originating from Mueller's wave function evolution in $1+3$ dimensions by resumming the leading logarithms in both large-Q^2 and large-rapidity $y = \ln\frac{1}{x}$, which we refer to as the DLA limit. We have shown that the hierarchy of moments allows for the reconstruction of a continuous probability distribution $f(z)$ supported in $(0,\infty)$, which is simply the KNO scaling function of the dipole multiplicity $p_n = \frac{1}{\bar{n}} f(\frac{n}{\bar{n}})$ with $z = \frac{n}{\bar{n}}$. The behavior of $f(z)$ at large and small z can be exactly determined, while the result for all values of z is only accessible numerically.

In principle, the virtual dipoles in the LFWF still need to pass through the final-state evolution stage to become real asymptotic states. However, the final-state evolution is less rapidity divergent, and we expect the main features of the dipole multiplicity distribution to hold. This distribution can be used as a probe for the final hadron multiplicities, as suggested in Refs. [29,51] (and references therein). Indeed, our parameter-free result reproduces well the DIS multiplicities reported by the H1 Collaboration at HERA in the highest Q^2 range; in particular, the observed KNO scaling function is in good agreement with the predicted dipole scaling function, including the overall shape, the location of the peak, and the large $z = \frac{n}{\bar{n}}$ tail. Our results show that the currently available DIS data at HERA are more amenable to the present DLA regime than to the diffusive or BFKL regime. The gluon multiplicities for both large and small $z = \frac{n}{\bar{n}}$ in the DLA regime should prove useful for more detailed comparisons with present and future DIS data, at large Q^2 and small parton-x. We have provided a pedagogical introduction to the leading-order BMS evolution equation and its relation to dipole evolution, from which the universality of the KNO scaling function is manifest.

The entanglement entropy in the DLA regime of DIS, is found to asymptote at $S = \ln\bar{n}$, much like in the diffusive (BFKL) regime. This is a general result of KNO scaling of the ensuing gluon multiplicities, satisfied by both regimes. However, the growth of the mean multiplicity $\bar{n} = xG(x,Q^2)$ is slower with $\bar{n} \sim e^{\#\sqrt{\alpha_s y}}$ or $S \sim \sqrt{\alpha_s y}$ in the DLA regime, and faster with $\bar{n} \sim e^{\#\alpha_s y}$ or $S \sim \alpha_s y$ in the BFKL regime. We regard this as an indication of faster scrambling of quantum coherence in the diffusive regime (smaller and smaller off-diagonal entries in the entangled density matrix). We emphasize that the entanglement entropy for DIS and jets in the DLA regime is directly accessible to current and future measurements.

Needless to say, the information encoded in the QCD multiplicities in the DLA regime is far more detailed than that captured by the entanglement entropy. However, the latter can be used as a sharp characterization of saturation, where the quantum cascade of dipoles reaches a state of maximum decoherence. Recall that a pure state with

maximal coherence carries zero entanglement entropy. But what is the signature for this onset, and what is its bound if any?

Saturation as a regime of maximal decoherence in the QCD cascade evolution of dipoles as gluons is likely to take place in the diffusive rather than the DLA regime, where the entanglement entropy is substantially larger with increasing rapidity. This is further supported by the observation that the diffusive multiplicities at weak coupling are very similar to the thermal distribution of a quantum oscillator. It is therefore not surprising that the same quantum entropy was noted in the dual string (a collection of quantum oscillators) exchanged between highly boosted hadrons (with emergent Unruh temperature). The dual string quantum entropy is extensive with the rapidity, commensurate with the transverse size growth of the boosted hadron as a stretched string, and saturates at one bit per string length squared [67]. These are the signature and bound we are looking for in characterizing the emitted hadronic multiplicities, as measured in both DIS and hadron scattering with large rapidity gaps. Remarkably, a similar signature and bound are observed in a classical black hole, where information is maximally scrambled on its near horizon and saturates to the lowest bound of one bit per Planck length squared [68].

ACKNOWLEDGMENTS

We are grateful to Jacek Wosiek for bringing to our attention Ref. [57] and to Yoshitaka Hatta for informing us about Refs [59,61]. This work is supported by the Office of Science, U.S. Department of Energy, under Contract No. DE-FG-88ER40388 and by the Priority Research Areas SciMat and DigiWorld under the program Excellence Initiative—Research University at the Jagiellonian University in Kraków.

APPENDIX: MULTIPLICITY DISTRIBUTIONS IN SUPER-RENORMALIZABLE THEORIES

In this appendix, we show in two examples that the multiplicity distribution in super-renormalizable theories (real or virtual), is in general Gaussian-like in the scaling region. This behavior is similar to the multiplicity distribution observed for the onium's LFWF in $1+2$D QCD [49]. In other words, KNO scaling holds only for critical theories with dimensionless couplings [31,69].

1. Ising model

The first example is the multiplicity distribution in the massive continuum limit of the 2D Ising model at zero magnetic field [70,71], where the mass of the free fermion equals m. We consider the spin-spin correlator $G(r)=\langle\Omega|\sigma(r)\sigma(0)|\Omega\rangle$ in its "form-factor expansion" [70–72]

$$G(r)=\sum_n\int\prod_i\frac{dp_i}{4\pi E_i}|\langle\Omega|\sigma(0)|p_1..p_n\rangle|^2e^{-r\sum_{i=1}^n E(p_i)}. \tag{A1}$$

The relative contribution from the n-particle sector can be regarded as a multiplicity distribution

$$\sigma_n(r)=\frac{1}{G(r)}\int\prod_i\frac{dp_i}{4\pi E_i}|\langle\Omega|\sigma(0)|p_1..p_n\rangle|^2e^{-r\sum_{i=1}^n E(p_i)}, \tag{A2}$$

with the normalization $\sum_n\sigma_n(r)=1$. To analyze this distribution at small $mr\ll 1$ or large energy $Q\gg m$, we consider the "lambda extension" [73]

$$G(r;\lambda)=\sum_n\lambda^n\int\prod_i\frac{dp_i}{4\pi E_i}|\langle\Omega|\sigma(0)|p_1..p_n\rangle|^2e^{-r\sum_{i=1}^n E(p_i)}, \tag{A3}$$

in terms of which the generating function for σ_n is

$$Z(\lambda,r)=\frac{G(r;\lambda)}{G(r)}. \tag{A4}$$

For $\lambda\leq 1$, $G(r;\lambda)$ has representation in terms of special solutions to Painlevé equations [70,73], with a small-r asymptotic [73,74]

$$G(r;\lambda)|_{r\to 0}=\tau_0(\sigma)(mr)^{-\frac{\sigma}{2}(1-\frac{\sigma}{2})}, \tag{A5}$$

where we have defined

$$\sigma\equiv\sigma(\lambda)=\frac{2}{\pi}\mathrm{Arcsin}(\lambda), \tag{A6}$$

$$\tau_0(\sigma)=Ae^{-3s^2\ln 2}\Gamma_2(1+s)\Gamma_2(1-s),\qquad s=\frac{1-\sigma}{2}. \tag{A7}$$

Here, $\Gamma_2(z)$ is the Barnes G function, and the value of the λ-independent constant A is not important. The mean multiplicity in the small-r limit follows as

$$\langle n\rangle=\frac{d}{d\lambda}Z(\lambda,r)|_{\lambda=1}\to\frac{2\ln\frac{8e^{\gamma_E+1}}{mr}}{\pi^2}+\mathcal{O}(mr\ln^2 mr)\sim\frac{2}{\pi^2}\ln\frac{1}{mr}, \tag{A8}$$

which is seen to grow logarithmically. On the other hand, the mean square deviation of the distribution reads

$$\sigma^2 = \langle n^2\rangle - \langle n\rangle^2 = \frac{d^2}{d^2\lambda} Z(\lambda, r)|_{\lambda=1} + \langle n\rangle - \langle n\rangle^2 \to \frac{4}{3\pi^2}\ln\frac{1}{mr} \sim \frac{2}{3}\langle n\rangle. \tag{A9}$$

Therefore, the width is of order $\sqrt{n}$, typical for a Poisson-like distribution. More specifically, we have

$$\lim_{r\to 0} Z\left(1-\frac{t}{\sigma}, r\right)\left(1-\frac{t}{\sigma}\right)^{-\langle n\rangle} = e^{\frac{t^2}{2}}, \tag{A10}$$

which implies

$$\sigma_n \to \frac{1}{\sigma} e^{-\frac{(n-\bar{n})^2}{2\sigma^2}}. \tag{A11}$$

The multiplicities fall into the Poisson universality class.

2. Phi-4

The second example is the ground-state wave function in terms of a free Fock basis in a super-renormalizable theory. As an example, consider a 2D free massive scalar field ϕ, supplemented by the quartic interaction term $H_I = g\int_{-\frac{L}{2}}^{\frac{L}{2}} :\phi^4(x):dx$. In the Fock basis of the free theory, the ground-state wave function of the interacting theory can be expanded as

$$|\Omega(L)\rangle = \sum_n p_n(L)|\Psi_n\rangle, \qquad \langle\Psi_n|\Psi_n\rangle = 1, \tag{A12}$$

where $p_n(L)$ is the probability of finding n particles of the free theory. As $L\to\infty$, the average particle number goes to infinity, and we would like to find out the distribution of p_n in this limit. For that, we introduce the generating function

$$Z(\lambda, L) = \sum_n \lambda^n p_n(L). \tag{A13}$$

In the large-L limit, as each connected diagram contributes a single factor of L, and the disconnected diagrams factorize (after summing over all time orderings), we have

$$Z(\lambda, L) = e^{-LF(1,g)} e^{LF(\lambda,g)}, \tag{A14}$$

where $LF(1,g)$ is the "field renormalization factor" for the vacuum. Here, $F(\lambda, g)$ is the sum over all the connected "real contributions" weighted over the number of particles in the "cut." Clearly, when $\lambda = 1$, $Z = 1$. For large L, we have

$$\bar{n} = L\left.\frac{dF(\lambda,g)}{d\lambda}\right|_{\lambda=1}, \tag{A15}$$

$$\sigma^2 = L\left.\frac{d^2F(\lambda,g)}{d^2\lambda}\right|_{\lambda=1} + L\left.\frac{dF(\lambda,g)}{d\lambda}\right|_{\lambda=1}. \tag{A16}$$

With this in mind, we can expand the generating function around $\lambda = 1$, with the result

$$\lim_{L\to\infty} Z\left(1-\frac{t}{\sigma}, L\right)\left(1-\frac{t}{\sigma}\right)^{-\langle n\rangle} = e^{\frac{t^2}{2}}. \tag{A17}$$

Again, this implies a Gaussian distribution for the limiting p_n.

[1] H. David Politzer, Reliable Perturbative Results for Strong Interactions?, Phys. Rev. Lett. **30**, 1346 (1973).
[2] David J. Gross and Frank Wilczek, Ultraviolet Behavior of Nonabelian Gauge Theories, Phys. Rev. Lett. **30**, 1343 (1973).
[3] J. D. Bjorken, Asymptotic sum rules at infinite momentum, Phys. Rev. **179**, 1547 (1969).
[4] Elliott D. Bloom *et al.*, High-Energy Inelastic ep Scattering at 6-Degrees and 10-Degrees, Phys. Rev. Lett. **23**, 930 (1969).
[5] Xiang-Dong Ji, Deeply virtual Compton scattering, Phys. Rev. D **55**, 7114 (1997).
[6] George F. Sterman, *An Introduction to Quantum Field Theory* (Cambridge University Press, Cambridge, England, 1993).
[7] John Collins, *Foundations of Perturbative QCD* (Cambridge University Press, Cambridge, England, 2013), Vol. 32.
[8] Alfred H. Mueller, Soft gluons in the infinite momentum wave function and the BFKL Pomeron, Nucl. Phys. **B415**, 373 (1994).
[9] Alfred H. Mueller, Unitarity and the BFKL Pomeron, Nucl. Phys. **B437**, 107 (1995).
[10] E. A. Kuraev, L. N. Lipatov, and Victor S. Fadin, The Pomeranchuk singularity in non-Abelian gauge theories, Sov. Phys. JETP **45**, 199 (1977).
[11] I. I. Balitsky and L. N. Lipatov, The Pomeranchuk singularity in quantum chromodynamics, Sov. J. Nucl. Phys. **28**, 822 (1978).
[12] L. N. Lipatov, Small-x physics in perturbative QCD, Phys. Rep. **286**, 131 (1997).
[13] I. Balitsky, Operator expansion for high-energy scattering, Nucl. Phys. **B463**, 99 (1996).
[14] Yuri V. Kovchegov, Small-x $F(2)$ structure function of a nucleus including multiple Pomeron exchanges, Phys. Rev. D **60**, 034008 (1999).

[15] Larry D. McLerran and Raju Venugopalan, Computing quark and gluon distribution functions for very large nuclei, Phys. Rev. D **49**, 2233 (1994).
[16] Larry D. McLerran and Raju Venugopalan, Gluon distribution functions for very large nuclei at small transverse momentum, Phys. Rev. D **49**, 3352 (1994).
[17] Edmond Iancu, Andrei Leonidov, and Larry McLerran, The color glass condensate: An introduction, in Cargese Summer School on QCD Perspectives on Hot and Dense Matter (2002), pp. 73–145, arXiv:hep-ph/0202270.
[18] Francois Gelis, Edmond Iancu, Jamal Jalilian-Marian, and Raju Venugopalan, The color glass condensate, Annu. Rev. Nucl. Part. Sci. **60**, 463 (2010).
[19] Leonard Susskind, String Theory and the Principles of Black Hole Complementarity, Phys. Rev. Lett. **71**, 2367 (1993).
[20] Leonard Susskind, Strings, black holes and Lorentz contraction, Phys. Rev. D **49**, 6606 (1994).
[21] Charles B. Thorn, Calculating the rest tension for a polymer of string bits, Phys. Rev. D **51**, 647 (1995).
[22] Mannque Rho, Sang-Jin Sin, and Ismail Zahed, Elastic parton-parton scattering from AdS/CFT, Phys. Lett. B **466**, 199 (1999).
[23] R. A. Janik and Robert B. Peschanski, Minimal surfaces and Reggeization in the AdS/CFT correspondence, Nucl. Phys. **B586**, 163 (2000).
[24] Joseph Polchinski and Matthew J. Strassler, Deep inelastic scattering and gauge/string duality, J. High Energy Phys. 05 (2003) 012.
[25] Richard C. Brower, Joseph Polchinski, Matthew J. Strassler, and Chung-I Tan, The Pomeron and gauge/string duality, J. High Energy Phys. 12 (2007) 005.
[26] Gokce Basar, Dmitri E. Kharzeev, Ho-Ung Yee, and Ismail Zahed, Holographic Pomeron and the Schwinger mechanism, Phys. Rev. D **85**, 105005 (2012).
[27] Alexander Stoffers and Ismail Zahed, Holographic Pomeron: Saturation and DIS, Phys. Rev. D **87**, 075023 (2013).
[28] V. Andreev *et al.* (H1 Collaboration), Measurement of charged particle multiplicity distributions in DIS at HERA and its implication to entanglement entropy of partons, Eur. Phys. J. C **81**, 212 (2021).
[29] E. Gotsman and E. Levin, High energy QCD: Multiplicity distribution and entanglement entropy, Phys. Rev. D **102**, 074008 (2020).
[30] Eugene Levin, Multiplicity distribution of dipoles in QCD from the Le-Mueller-Munier equation, Phys. Rev. D **104**, 056025 (2021).
[31] A. M. Polyakov, A similarity hypothesis in the strong interactions: 1. Multiple hadron production in e^+e^- annihilation, Zh. Eksp. Teor. Fiz. **59**, 542 (1970).
[32] Z. Koba, Holger Bech Nielsen, and P. Olesen, Scaling of multiplicity distributions in high-energy hadron collisions, Nucl. Phys. **B40**, 317 (1972).
[33] Yuri V. Kovchegov and Eugene Levin, *Quantum Chromodynamics at High Energy* (Cambridge University Press, Cambridge, England, 2012), Vol. 33.
[34] Alexander Stoffers and Ismail Zahed, Holographic Pomeron and entropy, Phys. Rev. D **88**, 025038 (2013).
[35] Dmitri E. Kharzeev and Eugene M. Levin, Deep inelastic scattering as a probe of entanglement, Phys. Rev. D **95**, 114008 (2017).
[36] Mark Srednicki, Entropy and Area, Phys. Rev. Lett. **71**, 666 (1993).
[37] Pasquale Calabrese and John L. Cardy, Entanglement entropy and quantum field theory, J. Stat. Mech. (2004) P06002.
[38] H. Casini, C. D. Fosco, and M. Huerta, Entanglement and alpha entropies for a massive Dirac field in two dimensions, J. Stat. Mech. (2005) P07007.
[39] M. B. Hastings, An area law for one-dimensional quantum systems, J. Stat. Mech. (2007) P08024.
[40] Pasquale Calabrese and John Cardy, Entanglement entropy and conformal field theory, J. Phys. A **42**, 504005 (2009).
[41] Edward Shuryak and Ismail Zahed, Regimes of the Pomeron and its intrinsic entropy, Ann. Phys. (Amsterdam) **396**, 1 (2018).
[42] Alex Kovner, Michael Lublinsky, and Mirko Serino, Entanglement entropy, entropy production and time evolution in high energy QCD, Phys. Lett. B **792**, 4 (2019).
[43] Silas R. Beane, David B. Kaplan, Natalie Klco, and Martin J. Savage, Entanglement suppression and Emergent Symmetries of Strong Interactions, Phys. Rev. Lett. **122**, 102001 (2019).
[44] John Arrington *et al.*, Opportunities for nuclear physics & quantum information science, in *Intersections between Nuclear Physics and Quantum Information*, edited by Ian C. Cloët and Matthew R. Dietrich (2019), arXiv:1903.05453.
[45] Nestor Armesto, Fabio Dominguez, Alex Kovner, Michael Lublinsky, and Vladimir Skokov, The color glass condensate density matrix: Lindblad evolution, entanglement entropy and Wigner functional, J. High Energy Phys. 05 (2019) 025.
[46] Dmitri E. Kharzeev, Quantum information approach to high energy interactions, Phil. Trans. A. Math. Phys. Eng. Sci. **380**, 20210063 (2021).
[47] Yizhuang Liu, Maciej A. Nowak, and Ismail Zahed, Entanglement entropy and flow in two dimensional QCD: Parton and string duality, Phys. Rev. D **105**, 114027 (2022).
[48] Adrian Dumitru and Eric Kolbusz, Quark and gluon entanglement in the proton on the light cone at intermediate x, Phys. Rev. D **105**, 074030 (2022).
[49] Yizhuang Liu, Maciej A. Nowak, and Ismail Zahed, Rapidity evolution of the entanglement entropy in quarkonium: Parton and string duality, Phys. Rev. D **105**, 114028 (2022).
[50] Peter J. Ehlers, Entanglement between valence and sea quarks in hadrons of $1+1$ dimensional QCD, Ann. Phys. (Amsterdam) **452**, 169290 (2023).
[51] Dmitri E. Kharzeev and Eugene Levin, Deep inelastic scattering as a probe of entanglement: Confronting experimental data, Phys. Rev. D **104**, L031503 (2021).
[52] Martin Hentschinski and Krzysztof Kutak, Evidence for the maximally entangled low-x proton in deep inelastic scattering from H1 data, Eur. Phys. J. C **82**, 111 (2022).
[53] Martin Hentschinski, Krzysztof Kutak, and Robert Straka, Maximally entangled proton and charged hadron multiplicity in deep inelastic scattering, Eur. Phys. J. C **82**, 1147 (2022).

[54] Krzysztof Kutak, Gluon saturation and entropy production in proton-proton collisions, Phys. Lett. B **705**, 217 (2011).
[55] Matthias Burkardt, Xiang-dong Ji, and Feng Yuan, Scale dependence of hadronic wave functions and parton densities, Phys. Lett. B **545**, 345 (2002).
[56] Yuri L. Dokshitzer, Victor S. Fadin, and Valery A. Khoze, On the sensitivity of the inclusive distributions in parton jets to the coherence effects in QCD gluon cascades, Z. Phys. C **18**, 37 (1983).
[57] Yuri L. Dokshitzer, Valery A. Khoze, Alfred H. Mueller, and S. I. Troian, *Basics of Perturbative QCD* (Editions Frontières, 1991), ISBN 9782863321010, https://www.google.pl/books/edition/Basics_of_Perturbative_QCD/GCROgr1CTjQC?hl=en&gbpv=0.
[58] A. Banfi, G. Marchesini, and G. Smye, Away from jet energy flow, J. High Energy Phys. 08 (2002) 006.
[59] Heribert Weigert, Nonglobal jet evolution at finite $N(c)$, Nucl. Phys. **B685**, 321 (2004).
[60] G. Marchesini and A. H. Mueller, BFKL dynamics in jet evolution, Phys. Lett. B **575**, 37 (2003).
[61] Yoshitaka Hatta and Takahiro Ueda, Resummation of non-global logarithms at finite N_c, Nucl. Phys. **B874**, 808 (2013).
[62] Simon Caron-Huot, Resummation of non-global logarithms and the BFKL equation, J. High Energy Phys. 03 (2018) 036.
[63] Lorenzo Cornalba, Eikonal methods in AdS/CFT: Regge theory and multi-Reggeon exchange, arXiv:0710.5480.
[64] Alexey A. Vladimirov, Correspondence between Soft and Rapidity Anomalous Dimensions, Phys. Rev. Lett. **118**, 062001 (2017).
[65] Tseh Liou, A. H. Mueller, and S. Munier, Fluctuations of the multiplicity of produced particles in onium-nucleus collisions, Phys. Rev. D **95**, 014001 (2017).
[66] D. Buskulic *et al.* (ALEPH Collaboration), Measurements of the charged particle multiplicity distribution in restricted rapidity intervals, Z. Phys. C **69**, 15 (1995).
[67] Yizhuang Liu and Ismail Zahed, Entanglement in Regge scattering using the AdS/CFT correspondence, Phys. Rev. D **100**, 046005 (2019).
[68] Jacob D. Bekenstein, Black holes and entropy, Phys. Rev. D **7**, 2333 (1973).
[69] J. Balog and M. Niedermaier, A Scaling Hypothesis for the Spectral Densities in the $O(3)$ Nonlinear Sigma Model, Phys. Rev. Lett. **78**, 4151 (1997).
[70] Tai Tsun Wu, Barry M. McCoy, Craig A. Tracy, and Eytan Barouch, Spin-spin correlation functions for the two-dimensional Ising model: Exact theory in the scaling region, Phys. Rev. B **13**, 316 (1976).
[71] Barry M. McCoy, Craig A. Tracy, and Tai Tsun Wu, Two-Dimensional Ising Model as an Exactly Solvable Relativistic Quantum Field Theory: Explicit Formulas for n Point Functions, Phys. Rev. Lett. **38**, 793 (1977).
[72] B. Berg, M. Karowski, and P. Weisz, Construction of Green functions from an exact S matrix, Phys. Rev. D **19**, 2477 (1979).
[73] Barry M. McCoy, Craig A. Tracy, and Tai Tsun Wu, Painleve functions of the third kind, J. Math. Phys. (N.Y.) **18**, 1058 (1977).
[74] Craig A. Tracy, Asymptotics of a tau function arising in the two-dimensional Ising model, Commun. Math. Phys. **142**, 297 (1991).